PCF BASED OPTICAL FIBER DESIGNING FOR SENSING IN TERAHERTZ SPECTRUM

by

Shaikh Rezwan (142466)
Md. Sharon Reza (142470)
Khalid Saifullah Uzzal (142485)
Md. Nafis Fuad (142486)

A Thesis Submitted to the Academic Faculty in Partial Fulfillment of the Requirements for the Degree of

BACHELOR OF SCIENCE IN ELECTRICAL AND ELECTRONIC ENGINEERING

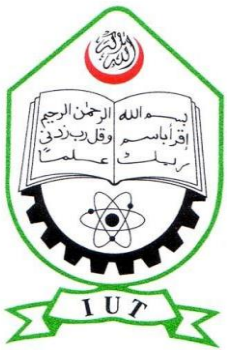

Department of Electrical and Electronic Engineering
Islamic University of Technology (IUT)
Gazipur, Bangladesh

November 2018

PCF BASED OPTICAL FIBER DESIGNING FOR SENSING IN TERAHERTZ SPECTRUM

Approved by:

Prof. Dr. Mohammad Rakibul Islam

Supervisor and Professor,
Department of Electrical and Electronic Engineering,
Islamic University of Technology (IUT),
Boardbazar, Gazipur-1704.

Date: ……

Table of Contents

ACKNOWLEDGEMENTS

The first thank and honor go to the Almighty. He has given us the capability and opportunity to finish this work perfectly. We have tried our best through the whole year and this research is our most significant scientific accomplishment in our educational life. But, without His help, it would not be possible for us.

After that, we would like to thank our honorable respected supervisor, Prof. Dr. Mohammad Rakibul Islam for his guidance, motivation and help during the thesis work. He has worked very hard and helped us a lot to finish and finalize this research work.

We would also like to thank other respective teachers, our friends and family members for their support and motivation which were also the key points behind our success.

ABSTRACT

Terahertz radiation occupies a middle ground between microwaves and infrared light waves known as the terahertz gap**,** where technology for its generation and manipulation is in its infancy. The frequency band of 0.1-10 THz, known as THz band has brought potential applications in many important fields. For wave propagation THz systems use free space as medium. But in free space waves face many difficulties which is very big issue for wave propagation. So, we have to use guided transmission instead of unguided transmission.

In the meantime, many guided transmission lines have many kinds of deprivation such as Effective Material Loss (EML), Confinement Loss, Bending Loss, Dispersion Loss, Power Fraction issue etc.

A highly sensitive porous core – photonic crystal fiber (PC-PCF) has been designed and analyzed for remote detection of chemical analytes in terahertz frequency range. The PC-PCF has been modelled using rectangular structured air holes in the core with square structured cladding. The full Vectorial finite Element Method (FEM) has been used to tune the geometrical parameters also to characterize the fiber.

At 1.8 THz, 37.3 μm slotted hole width and *x*-polarization mode the relative sensitivity for water, ethanol and benzene are 93.68%, 94.25%, and 94.43% respectively. The relative sensitivity obtained for the *y* polarization for water, ethanol and benzene are 94.4%, 94.92%, and 95.09% respectively. Effective Material Loss (EML) of water, ethanol benzene at frequency 1.8THz at x-polarization 0.06 cm^{-1}, 0.055 cm^{-1}, 0.054 cm^{-1} and at y-polarization 0.044 cm^{-1}, 0.0411 cm^{-1}, 0.054 cm^{-1} respectively. Effective area at optimum design parameters at x-polarization mode are 2.38E-07m^2, 2.25E-07m^2 and 2.21E-07m^2 at y-polarization mode are 2.38E-07m^2, 2.25E-07m^2 and 2.21E-07m^2 for water, ethanol and benzene respectively.

Simulation results demonstrate a high relative chemical sensitivity for different analytes. Moreover, the PCF shows very low near zero Dispersion Variation, high Modal Effective Area, high Birefringence and high Numerical Aperture (NA). The practical implementation of the fiber is feasible with the present fabrication techniques. The optimized PCF with such attractive characteristic has commercial applications in remote chemical sensing as well as polarization preserving applications of terahertz waves.

CHAPTER 1
INTRODUCTION

1.1 Optical Fiber Communication

Fiber optic communication is a communication technology that uses light pulses to transfer information from one point to another through an optical fiber. The information transmitted is essentially digital information generated by telephone systems, cable television companies, and computer systems.

1.2 Evolution of Fiber Optics Communication

Optical fiber was first developed in 1970 by Corning Glass Works. At the same time, GaAs semiconductor lasers were also developed for transmitting light through the fiber optic cables. The first-generation fiber optic system was developed in 1975, it used GaAs semiconductor lasers, operated at a wavelength of 0.8 μm, and bit rate of 45Megabits/second with 10Km repeater spacing.

In the early 1980's, the second generation of fiber optic communication was developed, it used InGaAsP semiconductor lasers and operated at a wavelength of 1.3 μm.

By 1987, these fiber optic systems were operating at bit rates of up to 1.7 Gigabits/second on single mode fiber with 50Km repeater spacing.

The third generation of fiber optic communication operating at a wavelength of 1.55 μm was developed in 1990. These systems were operating at a bit rate of up to 2.5 Gigabits/second on a single longitudinal mode fiber with 100Km repeater spacing.

The fourth generation of fiber optic systems made use of optical amplifiers as a replacement for repeaters, and utilized wavelength division multiplexing (WDM) to increase data rates. By 1996, transmission of over 11,300Km at a data rate of 5Gigabits/second had been demonstrated using submarine cables.

The fifth-generation fiber optic communication systems use the Dense Wave Division Multiplexing (DWDM) to further increase data rates. Also, the concept of optical solitons, which are pulses that can preserve their shape by counteracting the negative effects of dispersion, is also being explored.

1.3 Advancements

The major driving force behind the widespread use of fiber optics communication is the high and rapidly increasing consumer and commercial demand for more telecommunication capacity and internet services, with fiber optic technology capable of providing the required information capacity (larger than both wireless connections and copper cable). Advances in technology have enabled more data to be conveyed through a single optical fiber over long distances. The transmission capacity in optical communication networks are significantly improved using wavelength division multiplexing.

1.4 Contrivance

An optical network has the ability to process information entirely in the optical domain for the purpose of amplification, multiplexing, de-multiplexing, switching, filtering, and correlation, since optical signal processing is more efficient than electrical signal processing. Code Division Multiple Access networks using optical signal processing techniques have recently being introduced.

An optical fiber is a dielectric cylindrical waveguide made from low-loss materials, usually silicon dioxide. The core of the waveguide has a refractive index a little higher than that of the outer medium (cladding), so that light pulses is guided along the axis of the fiber by total internal reflection.

1.5 Fiber Transmission

Fiber optic communication systems consists of an optical transmitter to convert an electrical signal to an optical signal for transmission through the optical fiber, a cable containing several bundles of optical fibers, optical amplifiers to boost the power of the optical signal, and an optical receiver to reconvert the received optical signal back to the original transmitted electrical signal.

1.6 Basic Optical Fiber Communication System

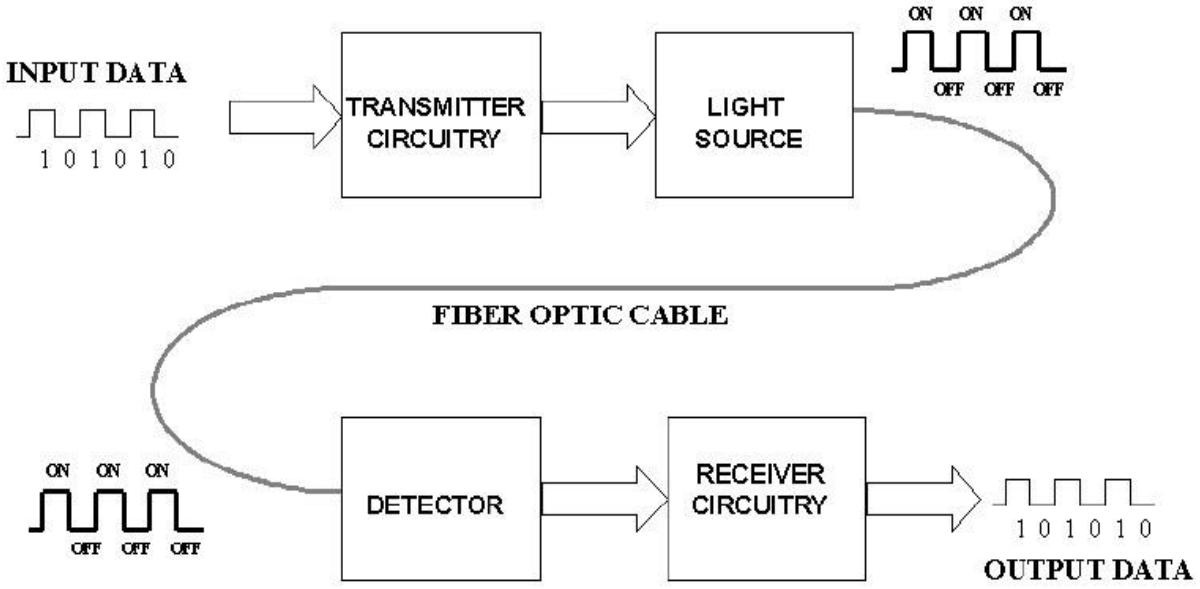

Fig 1.1: Basic fiber optic communication system

Figure 1.1 gives a simplified description of a basic fiber optic communication system.

1.7 Classification of Optical Fiber

Optical fibers fall into two major categories, namely:

i) Step index optical fiber
ii) Graded index optical fiber

1.7.1 Step index optical fiber

Step index optical fiber, which include single mode optical fiber and multimode optical fiber, and graded index optical fiber. Single mode step index optical fiber has a core diameter less than 10 micrometers and only allows one light path. Multimode step index optical fiber has a core diameter greater than or equal to 50 micrometers and allows several light paths, this leads to modal dispersion.

1.7.2 Graded index optical fiber

Graded index optical fibers have their core refractive index gradually decrease farther from the center of the core, this increased refraction at the core center slows the speed of some light rays, thereby allowing all the light rays to reach the receiver at almost the same time, thereby reducing dispersion.

1.8 Optical Fiber Modes

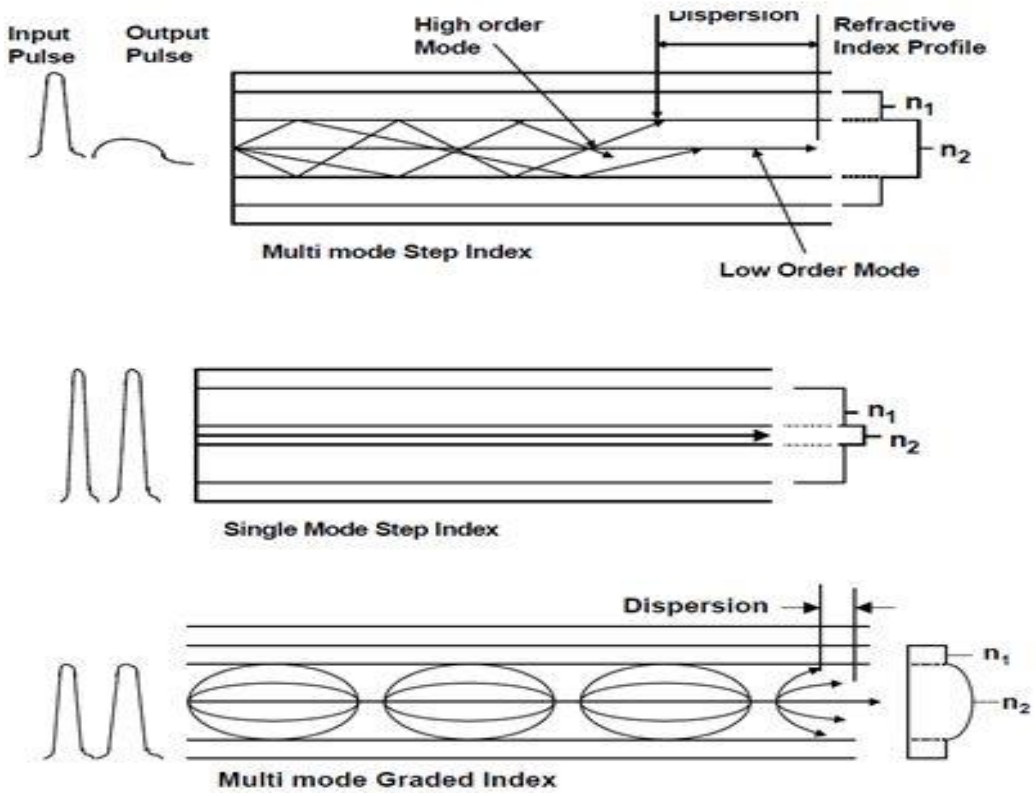

Fig 1.2: Optical Fiber Modes

Figure 1.2 gives a description of the various optical fiber modes.

1.9 Elementary Steps

The process of communicating using fiber-optics involves the following basic steps:

1. creating the optical signal involving the use of a transmitter, usually from an electrical signal
2. relaying the signal along the fiber, ensuring that the signal does not become too distorted or weak
3. receiving the optical signal
4. converting it into an electrical signal

Modern fiber-optic communication systems generally include an optical transmitter to convert an electrical signal into an optical signal to send into the optical fiber, a cable containing bundles of multiple optical fibers that is routed through underground conduits and buildings, multiple kinds of amplifiers, and an optical receiver to recover the signal as an electrical signal. The information transmitted is typically digital information generated by computers, telephone systems, and cable television companies.

1.9.1 Transmitters

The most commonly used optical transmitters are semiconductor devices such as light emitting (LEDs) and laser diodes. The difference between LEDs and laser diodes is that LEDs produce incoherent light, while laser diodes produce coherent light. For use in optical communications, semiconductor optical transmitters must be designed to be compact, efficient, and reliable, while operating in an optimal wavelength range, and directly modulated at high frequencies.

In its simplest form, an LED is a forward-biased p-n junction, emitting light through spontaneous emission, a phenomenon referred to as electroluminescence. The emitted light is incoherent with a relatively wide spectral width of 30-60 nm. LED light transmission is also inefficient, with only about 1% of input power, or about 100 microwatts, eventually converted into launched power which has been coupled into the optical fiber. However, due to their relatively simple design, LEDs are very useful for low-cost applications.

Today, LEDs have been largely superseded by VCSEL (Vertical Cavity Surface Emitting Laser) devices, which offer improved speed, power and spectral properties, at a similar cost. Common VCSEL devices couple well to multimode fiber.

1.9.2 Receivers

The main component of an optical receiver is a photodetector, which converts light into electricity using the photoelectric effect. The primary photodetectors for telecommunications are made from Indium gallium arsenide. The photo detector is typically a semiconductor-based photodiode. Several types of photodiodes include p-n photodiodes, p-i-n photodiodes, and avalanche photodiodes. Metal-semiconductor-metal (MSM) photo detectors are also used due to their suitability for circuit integration in regenerators and wavelength-division multiplexers.

Optical-electrical converters are typically coupled with a trans-impedance amplifier and a limiting amplifier to produce a digital signal in the electrical domain from the incoming optical signal, which may be attenuated and distorted while passing through the channel. Further signal processing such as clock recovery from data (CDR) performed by a phase-locked loop may also be applied before the data is passed on.

1.9.3 Transceiver

A transceiver is a device combining a transmitter and a receiver in a single housing. Most systems use a "transceiver" which includes both transmission and receiver in a single module. The transmitter takes an electrical input and converts it to an optical output from a laser diode or LED. The light from the transmitter is coupled into the fiber with a connector and is transmitted through the fiber optic cable plant. The light from the end of the fiber is coupled to a receiver where a detector converts the light into an electrical signal which is then conditioned properly for use by the receiving equipment.

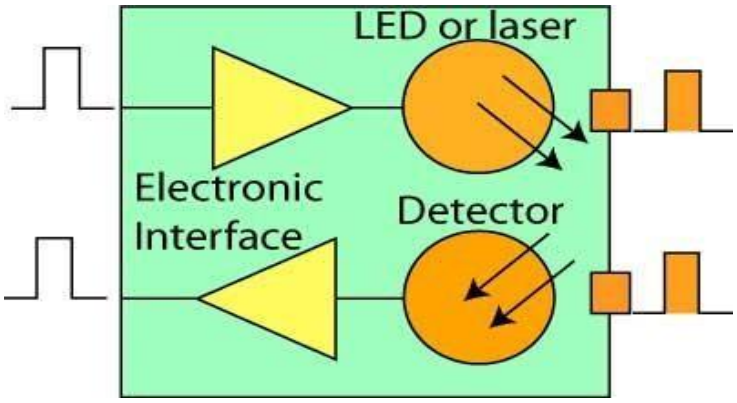

Fig 1.3: Fiber Optic Transceiver

1.9.4 Amplifier

The transmission distance of a fiber-optic communication system has traditionally been limited by fiber attenuation and by fiber distortion. By using opto-electronic repeaters, these problems have been eliminated. These repeaters convert the signal into an electrical signal, and then use a transmitter to send the signal again at a higher intensity than was received, thus counteracting the loss incurred in the previous segment.

Because of the high complexity with modern wavelength-division multiplexed signals (including the fact that they had to be installed about once every 20 km), the cost of these repeaters is very high.

1.10 Wavelength-Division Multiplexing

Wavelength-division multiplexing (WDM) is the practice of multiplying the available capacity of optical fibers through use of parallel channels, each channel on a dedicated wavelength of light. This requires a wavelength division multiplexer in the transmitting equipment and a demultiplexer (essentially a spectrometer) in the receiving equipment. Arrayed waveguide gratings are commonly used for multiplexing and demultiplexing in WDM. Using WDM technology now commercially available, the bandwidth of a fiber can be divided into as many as 160 channels to support a combined bit rate in the range of 1.6Tbit/s.

1.11 Applications of Optical Fiber

Optical fiber is used by many telecommunications companies to transmit telephone signals, Internet communication, and cable television signals. Due to much lower attenuation and interference, optical fiber has large advantages over existing copper wire in long-distance and high-demand applications. However, infrastructure development within cities was relatively difficult and time-consuming, and fiber-optic systems were complex and expensive to install and operate. Due to these difficulties, fiber-optic communication systems have primarily been installed in long-distance applications, where they can be used to their full transmission capacity, offsetting the increased cost. Since 2000, the prices for fiber-optic communications have dropped considerably.

The price for rolling out fiber to the home has currently become more cost-effective than that of rolling out a copper-based network. Prices have dropped to $850 per subscriber in the US and lower in countries like The Netherlands, where digging costs are low and housing density is high.

CHAPTER 2
DEVELOPMENT OF OPTICAL FIBER

In the recent years' THz wave generation and detection techniques have already been developed to cope with its popularity. However due to the lack of low loss transmission waveguides in the THz frequencies, most of the THz systems depends on free space for its wave propagation since all the remaining waveguides are extremely absorbent in this frequency band. Propagation in free space faces some undesirable problems. These include a tough configuration, path loss, an uncertain absorption loss influenced by the atmosphere, and difficult integration with other components. Therefore, transmissions of THz waves for long distance are still in the demanding state.

Therefore, much effort has been given for its solutions, one can be to use optical fiber where there is no influence of external free space, these can dramatically reduce the losses and alignment problems also the system performances can also be increased.

2.1 Terahertz Frequency Range

The TERAHERTZ (THz) frequency/wavelength window of the electro-magnetic spectrum lies between the infrared band and the microwave banded ranges in frequency from 0.1 to 10 THz (equivalently wavelength ranges from 3 mm – 30 μm). Radiation from any object with temperature > 10 K contains THz wavelengths and almost 98% of cosmic background radiations since Big-Bang event corresponds to THz and far-infrared frequencies. Initially THz radiation was mainly used for passive applications, where THz waves were detected to study the chemistry of cold planetary atmosphere and interstellar medium.

This frequency range can transfer huge data files via wireless route and can significantly increase the communication data rate over existing microwave technology. THz waves can deeply penetrate through cloths, ceramics, walls, woods, paper, dry air, polymers etc., but they are absorbed or reflected by metal, water vapor, dust, cloud, and sufficiently dense objects. Additionally, THz

waves are also not harmful to human health. All these excellent qualities of THz radiation make it suitable for imaging of hidden objects, like explosives, metallic weapons etc. Most importantly, this technology has already begun to make deep inroads in non-invasive medical diagnostics, such as detection of skin cancer, tooth decay, and identification of human tissues based on different refractive indices and linear absorption coefficients at THz frequencies.

2.2 Wave Propagation

Since most of the THz systems and THz communication experiments are bulky and are performed in free space, it faces many undesirable problems. These include a tough transmitter-receiver alignment issues, an uncertain absorption loss influenced by the surroundings and difficult integration with other components.

To overcome these problems, researchers proposed guided transmission instead of unguided transmission. Researchers showed that the THz wave can nicely be propagated through all kinds of conventional metallic waveguides.

2.3 Backdrop to THz Waveguides

In the early 1980s, THz pulses (in the pico/sub picosecond regime) were generated and sampled by photoconductive switches, also known as Auston switches. These photoconductive switches were incorporated into microstrip and coplanar (still used today) transmission lines.

A microstrip transmission line is a type of electrical transmission line that consists of a conducting strip separated from a ground plane by a dielectric substrate, while a coplanar transmission line is an alternative type of electrical transmission line that consists of a conducting strip on a dielectric substrate with two ground electrodes running adjacent and parallel to strip.

A limitation of the microstrip line configuration, in the THz system, was that such systems suffered from reflections (ringing) at the generation point. Also, these microstrip based THz systems had high dispersion due to the dielectric substrate.

In the coplanar transmission THz system, the generated sub picosecond pulse (0.6 ps, for example) undergoes lower distortion compared to microstrip lines. Therefore, they are more suitable for far-IR spectroscopy.

The coplanar transmission line THz system suffers from strong frequency dependent loss due to Cherenkov-like radiation, which is equivalent to the loss process of leaky waveguides in the frequency domain. The total observed loss owing to the dielectric and metal in microstrip and coplanar transmission lines in THz systems is very high.

For thin-film microstrip and coplanar transmission lines are $\alpha = 18\ cm^{-1}$ and $\alpha = 14\ cm^{-1}$ at 1 THz, respectively. The loss increases as frequency increases with f and f^3 dependence, respectively.

Initially, to propagate THz wave researchers used Circular metallic waveguide [1] like stainless solid but these waveguides are highly lossy on the order of 50 DB/cm. Although a THz wave cannot be guided inside a hollow dielectric tube, if this tube is coated with a metal layer, a plasmonic mode can form inside the hollow core, where the guiding environment can be better controlled or manipulated.

It has been observed that by incorporating an additional thin dielectric layer [2], the mode field can be drawn away from the lossy plasmonic interface and, as a consequence, the overall loss value can be reduced [3]. However, these waveguides are not very flexible for large diameter waveguides and increase the loss value for small diameter waveguides.

Hollow dielectric tubes [4] coated with metal layer were reported, but they appeared to be bulky.

To overcome these obstacles, one usually designs various kinds of waveguides to guide the THz wave because the material absorption loss is high in THz band. One of the lowest material loss materials is dry air in the THz frequency range. It has been reported [5] that the mode field extends into the low index air cladding region when a dielectric rod is surrounded by air and is operating very close to its cutoff frequency. The main disadvantage of this design is that the mode extends considerably into the surrounding air cladding and the power is propagated mostly outside the waveguide, which strongly interacts with the surrounding environment. As a result, the bending loss would also be expected to be excessively high.

Plastic sub wavelength fibers [6] came into existence for their comparatively lower losses. However, there is a disadvantage for the sub-wavelength fibers that most of the field propagates outside the waveguide core, thus resulting in strong coupling to the environment.

For improvement, Nagel et al. [7] reported the addition of a sub-wavelength hole within a solid core, which increases the guided field in the air hole and hence reducing the absorption losses. However, the loss due to the material is still high.

2.4 Use of Polymers for THz Wave Guiding

Interest of researchers shifted from dielectrics to polymers when Chen et al. [8] showed that polyethylene can be used as a guidance material which has lower absorption loss. In recent times, variety of polymers such as Polymethyl Methacrylate (PMMA) [9], TOPAS [10], Teflon [11] etc. are being used as primary choices for THz wave guiding.
In order to reduce absorption loss further, researchers put their attention into guiding structure designing. Dry air is assumed to have no material absorption loss at THz frequency range. On the basis of that, wave guide with sub-wavelength air hole in the core was reported [8]. However, it caused huge power dissipation outside the guide. Later, polystyrene foam was introduced [12] which had a major disadvantage that it required larger dimension.

Actually, genuine breakthrough of the research works occurred when polymer materials were used instead of metals in the background which represent a much lower absorption loss.

2.4.1 Hollow core Bragg Fiber

Hollow core Bragg fibers [13-14] have also been considered which, unfortunately, had unwanted narrow band properties.

2.4.2 Photonic Crystal Fiber

Photonic crystal fiber (PCF) is the most popular optical fiber but in case of a solid core [15], the material absorption loss is too high and is almost equal to the bulk absorption loss of the material.

In a PCF, light is guided through the waveguide using total internal reflection property based on the difference between refractive indices of the core and the cladding. In general, the cladding is consisted of a number of air holes [16]. Recently, PCFs have been popular for their modification enabled property which helps controlling their behavior. Although, solid core polymer-made PCFs had been introduced for THz wave guiding, [11, 17] they could not create a spark because the solid core caused significant amount of loss. As an attempt, air filling ratio was extremely increased to force the light through air holes of the cladding [18-19], but size of the waveguide got enlarged.

2.5 Use of Porous Air Core in PCF

Implementing porous air core in a PCF instead of solid rod came out as a solution. Use of a porous core is resulted in reduction of quantity of solid material in the core as well as the absorption loss.

2.5.1 Honeycomb Band-gap Fibers

Efficient honeycomb band-gap fibers were reported [20-21], where porous core PCFs were investigated both numerically and experimentally. Also, a hexagonal PCF with hexagonal porous core was reported [22] with a low absorption loss (0.12 cm^{-1}) where Teflon was used as the background material.

2.5.2 Sub-wavelength Porous Fibers

The sub-wavelength porous fibers have been proven to exhibit some merits namely extremely low loss, design and fabrication flexibilities, and small fiber diameters [23].
Moreover, dispersion of the porous fibers can be controlled easily. In such fibers, owing to the sub-wavelength diameter of the core, the fundamental guided mode presents surrounding the air-cladding and hence low absorption loss is obtained [24].

2.5.3 Use of Topaz

A better approach with TOPAS was presented which had an octagonal porous core inside an octagonal cladding [25] with a lower loss (0.07 cm^{-1}) resulted due to the lower bulk material absorption loss of TOPAZ. Nevertheless, the paper had no discussion on power fraction or dispersion properties.

CHAPTER 3
PCF IN TERAHERTZ SPECTRA

3.1 Contextual Overview of Optical Fibers

Various porous core PCFs with noticeable material loss properties were reported over the ages. A microstructure core honeycomb band-gap fiber for THz wave guidance was reported by Neilsen et al. [26] but in this case periodicity still needs to be maintained strictly in narrowband fibers to satisfy the Bragg conditions.

Porous core fiber with TOPAS as background material using hexagonal structure in both core and cladding was reported by Uthman et al. [27] reported which showed Effective Material Loss (EML) of 0.12 cm-1 but they didn't mention some important properties for THz applications like dispersion and fraction of power.

A porous core fiber having both flattened dispersion and 80% light confinement within the core area was proposed by Liang et al. [28] Because of having higher absorption loss of 0.432 dB/cm at 1.0 THz, this design has not been so seductive for THz guidance.

Kaijage et al. [29] reported a porous core fiber which warrants effective material loss of 0.076 cm-1 but they did not take into consideration some crucial design issues for THz guidance such as dispersion and core power fraction.

A fiber with hexagonal core and rotate hexagonal cladding was proposed by Islam et al. [30] which showed the EML= 0.066 cm-1 and core power fraction of 0.40.

A fiber with octagonal core and cladding structure was proposed by Rana et al. [31] but it showed a material loss of 0.058 cm-1 and they neglect to investigate the dispersion properties of that fiber.

A fiber with octagonal structure in the cladding and circular structure in the core was proposed by Hasan et al. [32] which showed an effective material loss of 0.056 cm-1 but they didn't even mention the single mode condition which is one of the main properties for analyzing a fiber.

A rotated hexagonal core surrounded by a circular shape cladding was reported by Saiful et al. [33] which gave loss of .053 cm-1 but can be further reduced & thus improve the efficiency.

3.2 Photonic-Crystal Fiber

Photonic-crystal fiber (PCF) is a new class of optical fiber based on the properties of photonic crystals. Because of its ability to confine light in hollow cores or with confinement characteristics not possible in conventional optical fiber, PCF is now finding applications in fiber-optic communications, fiber lasers, nonlinear devices, high-power transmission, highly sensitive gas sensors, and other areas. More specific categories of PCF include photonic-bandgap fiber (PCFs that confine light by band gap effects), holey fiber (PCFs using air holes in their cross-sections), hole-assisted fiber (PCFs guiding light by a conventional higher-index core modified by the presence of air holes), and Bragg fiber (photonic-bandgap fiber formed by concentric rings of multilayer film).

Photonic crystal fibers may be considered a subgroup of a more general class of micro structured fibers, where light is guided by structural modifications, and not only by refractive index differences.

3.2.1 Classification of PCF

Optical fibers have evolved into many forms since the practical breakthroughs that saw their wider introduction in the 1970s as conventional step index fibers and later as single material fibers where propagation was defined by an effective air cladding structure.

In general, regular structured fibers such as photonic crystal fibers, have a cross-section (normally uniform along the fiber length) micro-structured from one, two or more materials, most commonly arranged periodically over much of the cross-section, usually as a "cladding" surrounding a core (or several cores) where light is confined. For example, the fibers first demonstrated by Russell consisted of a hexagonal lattice of air holes in a silica fiber, with a solid (1996) or hollow (1998) core at the center where light is guided. Other arrangements include concentric rings of two or more materials, first proposed as "Bragg fibers" by Yeh and Yariv (1978), a variant of which was recently fabricated by Temelkuranet al. (2002) and others.

(Note: PCFs and, in particular, Bragg fibers, should not be confused with fiber Bragg gratings, which consist of a periodic refractive index or structural variation along the fiber axis, as opposed to variations in the transverse directions as in PCF. Both PCFs and fiber Bragg gratings employ Bragg diffraction phenomena, albeit in different directions.

The lowest reported attenuation of solid core photonic crystal fiber is 0.37 dB/km, and for hollow core is 1.2 dB/km.

3.2.2 Composition of PCF

Generally, such fibers are constructed by the same methods as other optical fibers: first, one constructs a "preform" on the scale of centimeters in size, and then heats the preform and draws it down to a much smaller diameter (often nearly as small as a human hair), shrinking the preform cross section but (usually) maintaining the same features. In this way, kilometers of fiber can be produced from a single preform. The most common method involves stacking, although drilling/milling was used to produce the first aperiodic designs. This formed the subsequent basis for producing the first soft glass and polymer structured fibers.

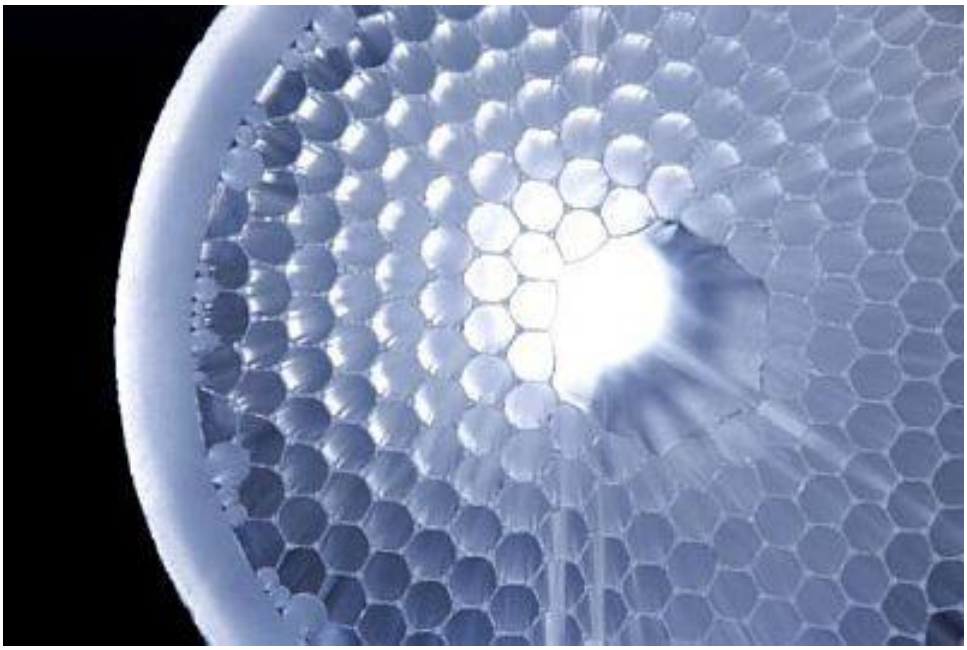

Fig 3.1: Photonic Crystal Fiber

Most photonic crystal fibers have been fabricated in silica glass, but other glasses have also been used to obtain particular optical properties (such as high optical non-linearity). There is also a growing interest in making them from polymer, where a wide variety of structures have been explored, including graded index structures, ring structured fibers and hollow core fibers. These polymer fibers have been termed "MPOF", short for micro-structured polymer optical fibers (van Eijkelenborg, 2001). A combination of a polymer and a chalcogenide glass was used by Temelkuranet al. (2002) for 10.6 μm wavelengths (where silica is not transparent).

3.2.3 Modes of operation of PCF

Photonic crystal fibers can be divided into two modes of operation, according to their mechanism for confinement. Those with a solid core, or a core with a higher average index than the micro-structured cladding, can operate on the same index-guiding principle as conventional optical fiber — however, they can have a much higher effective- refractive index contrast between core and cladding, and therefore can have much stronger confinement for applications in nonlinear optical devices, polarization maintaining fibers, (or they can also be made with much lower effective index contrast). Alternatively, one can create a "photonic bandgap" fiber, in which the light is confined by a photonic bandgap created by the micro-structured cladding – such a bandgap, properly designed, can confine light in a lower-index core and even a hollow (air) core. Bandgap fibers with hollow cores can potentially circumvent limits imposed by available materials, for example to create fibers that guide light in wavelengths for which transparent materials are not available (because the light is primarily in the air, not in the solid materials). Another potential advantage of a hollow core is that one can dynamically introduce materials into the core, such as a gas that is to be analyzed for the presence of some substance. PCF can also be modified by coating the holes with sol-gels of similar or different index material to enhance its transmittance of light.

3.3 The THz Band Spectra

Terahertz radiation falls in between infrared radiation and microwave radiation in the electromagnetic spectrum and it shares some properties with each of these. Like infrared and microwave radiation, terahertz radiation travels in a line of sight and is nonionizing. Like microwave radiation, terahertz radiation can penetrate a wide variety of non-conducting materials. Terahertz radiation can pass through clothing, paper, cardboard, wood, masonry, plastic and ceramics. The penetration depth is typically less than that of microwave radiation. Terahertz radiation has limited penetration through fog and clouds and cannot penetrate liquid water or metal.

In physics, terahertz radiation, also called submillimeter radiation, terahertz waves, terahertz light, T-rays, T-waves, T-light, T-lux, or THz, consists of electromagnetic waves at frequencies from 0.3 to 10 terahertz (THz). The term applies to electromagnetic radiation with frequencies between the high-frequency edge of the millimeter wave band, 300 GHz and the low frequency edge of the far-infrared light band, 3000 GHz. Corresponding wavelengths of radiation in this band range from 1 mm to 0.1 mm (or 100 μm). Because terahertz radiation begins at a wavelength of 1 mm and

proceeds into shorter wavelengths, it is sometimes known as the submillimeter band and its radiation as submillimeter waves, especially in astronomy.

The earth's atmosphere is a strong absorber of terahertz radiation in specific water vapor absorption bands, as seen in Fig 3.2, so the range of terahertz radiation is limited enough to affect its usefulness in long-distance communications. However, at distances of ∼10 m the band may still allow many useful applications in imaging and construction of high bandwidth wireless networking systems, especially indoor systems.[3] In addition, producing and detecting coherent terahertz radiation remains technically challenging, though inexpensive commercial sources now exist in the 300–1000 GHz range (the lower part of the spectrum), including gyrotrons, backward wave oscillators, and resonant-tunneling diodes.

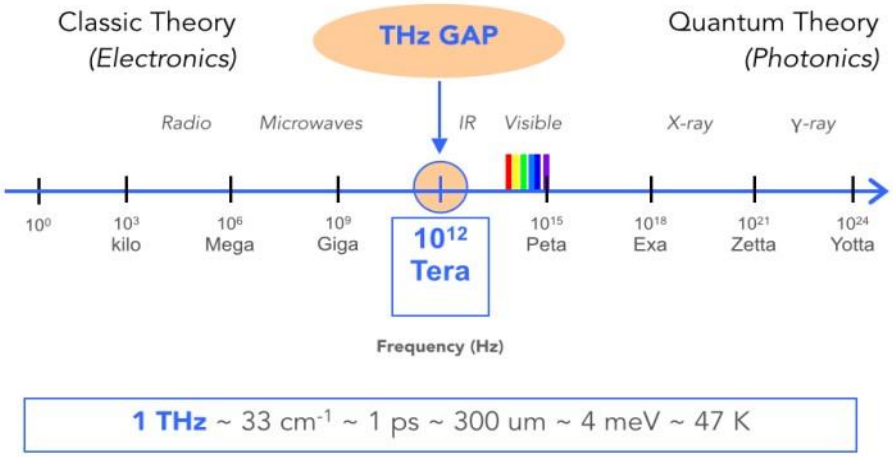

Fig 3.2: THz gap in electromagnetic spectrum

Terahertz radiation occupies a middle ground between microwaves and infrared light waves, and technology for generating and manipulating it is in its infancy and is a subject of active research (Fig. 1). It represents the region in the electromagnetic spectrum in which the frequency of electromagnetic radiation becomes too high to be measured by directly counting cycles using electronic counters, and must be measured by the proxy properties of wavelength and energy.

Similarly, in this frequency range the generation and modulation of coherent electromagnetic signals ceases to be possible by the conventional electronic devices used to generate radio waves and microwaves, and requires new devices and techniques. The electromagnetic range that is used is very vast. At low frequencies end we have radio waves up to millimeter waves, and at the other

end we have optical waves down to the far infrared. Technologies have been developed for both ends of the spectrum which we use in everyday applications. But the terahertz region:

0.3-10THz, 1THz=1012Hz

With wavelength of 30 μm^{-3} mm has remained largely underdeveloped, despite the identification of various applications, in particular terahertz imaging and others which will be discussed later on.

It is possible to produce effectively radiation in the low frequency region (microwaves) with oscillating circuits based on high-speed transistors and at high frequencies (visible spectrum) with semiconductor lasers. But transistors and other electric devices based on electric transport have in principle a limit at about 300 GHz, but are practically limited to about 50 GHz, because devices above this are extremely inefficient and the frequency of semiconductor lasers can only be extended down to about 30 THz. Thus, there is a region in between where both technologies do not meet. This region is often referred to as the terahertz gap.

Terahertz radiations have a few remarkable properties. Many common materials and living tissues are semitransparent and have 'terahertz fingerprints', permitting them to be imaged, identified and analyzed. Due to non-ionizing properties of terahertz radiations are safe for screening application. These unique properties of radiations are now exploited due to availability of commercial sources of terahertz radiations.

Pharmaceutical Industry: Tablet Integrity and Performance:

Coating has a wide variety of functions. The most important function of coating is to regulate the controlled release of active ingredients in the body. Coating not only contributes to the bioavailability of a particular drug or combination of drugs during certain times and locations but also coating can protect the stomach from high concentrations of active ingredients, improve tablet visual appeal and extend shelf life by protecting the ingredients from degradation by moisture and oxygen. In relation to tablet coating the process analytical technology (PAT) initiative is intended to improve consistency and predictability of tablet action by improving quality and uniformity of tablet coatings. Issues with coating can arise from problems with the coating materials or flaws in the coating pan or spray process. If a coating is non-uniform or has surface defects then the desired dose delivery and bioavailability can be compromised. From this standpoint it is important to characterize tablet coating uniformity, both within a single tablet and across an entire batch to develop an understanding of the functional analysis of the final product. Several analytical and imaging techniques are being used to understand the critical processes involved in tablet coating

but none of them is ideal to fully characterize the layers. Some of the techniques that provide useful information are atomic force microscopy, confocal laser microscopy, X-ray photoelectron spectroscopy, electron paramagnetic resonance, Fourier transform infrared spectroscopy, and laser induced breakdown spectroscopy (LIBS) and scanning thermal microscopy. However, all these methods are either destructive to the tablet or cannot be readily implemented for rapid on-line measurement.

Terahertz image can be optimized for performing 3D analysis on tablets. It can enable to determine coating integrity and thickness, detect and identify localized chemical or physical structure such as cracks or chemical agglomeration within a core and to interrogate embedded layers (such as an interface between two layers) for delamination and integrity. Terahertz measurements may well become the primary method for the nondestructive determination of coating thickness, requiring little or no calibration for most coatings and substrates. It can reveal the thickness, uniformity, distribution and coverage of simple and complex coating. Terahertz image can also detect embedded layers and localized chemical or physical structural features in the cores of intact tablets to confirm 3D morphology and blend uniformity.

Terahertz pulsed imaging (TPI)

TPI is a completely non-invasive and non-destructive pharmaceutical analysis tool using extremely low power, ultra-short pulses of electromagnetic radiation at lower frequencies than infrared (1 THz = 1012 Hz). Terahertz spectroscopy has already proved useful to distinguish between different polymorph forms of the drug. TPI is a next step of this whereby THz pulses are used to image object of interest. THz pulses are generated by illuminating photoconductive semi-conductors with pulsed near-infrared laser radiation and detected coherently. Tablet coatings are semi-transparent to THz frequencies and do no scatter them significantly. THz pulses incident on a tablet surface penetrate through the different coating layers. At each interface a portion of THz radiations is reflected back to the detector. The amplitude of reflected THz radiation is recorded as a function of time. In this technique the sample itself is completely unaffected by the measurement. Coating thickness uniformity is established simply from the transit time of the pulse to each interface. With knowledge of the refractive index of coating material the actual thickness can be determined to a depth resolution of about 20 microns. The spot size of the THz pulse, and therefore lateral resolution, is about 250 microns.

Molecular structure

The sensitivity and specificity of terahertz spectroscopy to both intermolecular and intramolecular vibrations in different chemical species enable investigation of the crystalline state of drugs e.g. Polymorphism. The use of pulsed terahertz imaging in proteomics and drug discovery determines protein 3D structure, folding and characterization. It is also very sensitive to DNA hybridization and other interactions. Terahertz spectroscopy provides rapid identification of the different crystalline forms of drug molecules – the polymorphs – which can exhibit different solubility's, stabilities and bioavailability and hence are an important factor in the therapeutic efficacy of a drug. Detecting and identifying the different polymorphs and understanding the mechanism and dynamics of polymorphic inter-conversion, is an important milestone in selecting the optimum form for further development and manufacture. It is possible not only to detect the differences between pure specimens of the polymorphs but terahertz spectroscopy can distinguish between specific polymorphic forms in tablet formulation.

Terahertz spectroscopy can also differentiate between different hydrate forms. Lactose which is one the most commonly used excipients in the pharmaceutical industry has at least three different hydrates namely α-monohydrate, α-anhydrate and β-anhydrate form. These three hydrate forms exhibit terahertz spectra that can be used for both quantitative and qualitative analysis. Terahertz region provides unique sensitivity to lattice structure enabling qualitative and qualitative analysis of crystalline and amorphous materials as well.

Time Resolved THz Spectroscopy of Protein Folding

Proteins fold, catalyze reactions, and transducer signals via binding to other biomolecules. These processes are driven by motions with characteristics time scales ranging from femtoseconds (fs) to milliseconds (ms). The characteristic modes from which such motions collectively emerge often cause large amplitude deformations of all or part of the protein. Temperature tuning reveals when certain modes are frozen out, while the terahertz spectroscopy can cover fast relaxation kinetics on fs time scale during which a protein rearranges its overall structure.

In Dermatology

The cosmetic appearance of skin is directly linked to the outermost layer, the stratum corneum. The water content of the stratum corneum influences its permeability and elasticity. Most skin-care products such as moisturizers act to increase the retained water content of this layer of the skin to enhance its appearance. Quantitative characterization of the hydration level of the stratum corneum is thus of crucial importance to the cosmetic industry in order to characterize and compare the effectiveness of their products.

Basal cell carcinoma (BCC) is the most common form of cancer worldwide in white populations and has a reported annual incidence of over 1 million in the U.S.A. Several different imaging techniques are being evaluated as diagnostic tools for skin lesions and tumor margin assessment. The terahertz (THz) frequency wavelength is of particular interest as it excites the intermolecular interactions, such as the liberational and vibrational modes of molecules providing spectroscopic information. Terahertz pulse imaging (TPI) is a noninvasive, coherent optical imaging modality that explores this frequency region. These wavelengths are significantly larger than the scattering structures in tissue; therefore, we assume that scattering effects are negligible. The current lateral and axial resolutions attainable with our system at 1 THz are 350 m and 40 m, respectively, making it a viable imaging modality. As TPI is a coherent, time gated, low noise technique, both phase and amplitude information can be obtained, from which the absorption and refractive index of a medium can be determined. This enables TPI to provide both structural and functional information, due to chemical specificity. Through examination of the terahertz waveform in both the time and frequency domains, TPI may prove advantageous in distinguishing type, lateral spread, and depth of tumors.

Oral Healthcare

Dental carries or tooth decay is one of the most common human disorders. Carries proceed by the creation of a subsurface lesion in the enamel. The lesion may extend to the next tissue in the layer in teeth, the dentine, without macroscopically visible breakdown or even microcavity formation at the tooth surface. The absence of visual features on the tooth surface makes early detection of tooth decay difficult. X-rays which is one of the accepted methods used to detect decay, only reveals the problem at a relatively late stage, when drilling and filling is the only method available to halt the decay. If decay can be detected early enough it is possible to reverse the process without the need for drilling by the use of either fissure sealing or remineralization.

Terahertz imaging can distinguish between the different types of tissue in a human tooth; detect carries at an early stage in the enamel layers of human teeth and monitor early erosion of the enamel at the surface of the tooth.

Oncology

It is estimated that more than 85% of all cancers originate in the epithelium. Excision biopsy to remove tissue from the body and examining it under a microscope is the gold standard for cancer diagnosis. Terahertz technology has the potential to greatly improve conventional biopsy and associated surgery by more precisely identifying the areas to be excised thereby reducing the number of procedures and facilitating earlier and more accurate diagnosis. As the technology develops, it may be possible to perform biopsies using live terahertz imaging of affected area, making possible point of care optical biopsy.

Detection of Impurities in Pharmaceutical Industry

The manufacturing of pharmaceutical products is a highly monitored process that requires strict quality regulations. If the final product fails to meet the standard set by regulatory agencies then the whole batch is destroyed. This encourages the pharmaceutical industry to work on batch-processing techniques. Typically, pharmaceutical companies manufacture a finished product and then use laboratories to analyze a proportion of the batch to verify the quality of their product.

Terahertz radiation has the ability to obtain information on chemical and physical structures and is able to accomplish this in real-time in a non-destructive form. This shows potential for the pharmaceutical industry as it is able to specifically determine the structure and properties of the sample to test, such as the bioavailability, manufacturability, purification, stability, dissolution rate, solubility and other performance characteristics of the drug. During manufacturing, solid pharmaceutical materials may come into contact with water or other impurities during processing, which can affect the product performance. THz Spectroscopy can measure the unique physico-chemical properties of a product, being able to specifically distinguish one product from another which provides quality information. Terahertz Spectroscopy can also be used to patent pharmaceutical products because of the ability to distinguish the specific chemical components.

Medical Imaging

Contrary to X-rays, terahertz radiation has relatively low photon energy for damaging tissues and DNA. Some frequencies of terahertz radiation can penetrate several millimeters of tissue with low water content (e.g., fatty tissue) and reflect back.

Terahertz radiation can also detect differences in water content and density of a tissue. Such methods could allow effective detection of epithelial cancer with an imaging system that is safe, non-invasive, and painless.

Spectroscopy in terahertz radiation could provide novel information in chemistry and biochemistry. Recently developed methods of THz time-domain spectroscopy (THz TDS) and THz tomography have been shown to be able to perform measurements on, and obtain images of, samples that are opaque in the visible and near-infrared regions of the spectrum. The utility of THz-TDS is limited when the sample is very thin, or has a low absorbance, since it is very difficult to distinguish changes in the THz pulse caused by the sample from those caused by long-term fluctuations in the driving laser source or experiment. However, THz-TDS produces radiation that is both coherent and spectrally broad, so such images can contain far more information than a conventional image formed with a single-frequency source.

Security

Terahertz radiation can penetrate fabrics and plastics, so it can be used in surveillance, such as security screening, to uncover concealed weapons on a person, remotely. This is of particular interest because many materials of interest have unique spectral “fingerprints” in the terahertz range. This offers the possibility to combine spectral identification with imaging. Passive detection of terahertz signatures avoids the bodily privacy concerns of other detection by being targeted to a very specific range of materials and objects.

At airports or other security critical places dangerous non-metallic substances like ceramic knifes or plastic explosives now can be detected with terahertz beams. This is possible because T-rays get through clothes, but cannot get through the upper skin (because of the water content.

Communication

Potential uses exist in high-altitude telecommunications, above altitudes where water vapor causes signal absorption: aircraft to satellite, or satellite to satellite.

3.4 Overview of Some Important Background Work Done in Different Times:

- A polarization maintaining ultra-low effective material loss based on slotted core kagome lattice fiber is proposed for terahertz (THz) wave propagation was proposed by Md Rabiul Hasan, Numerical study demonstrates that by using rectangular slotted air holes in the core of the kagome lattice exhibits simultaneously an ultra-high birefringence of $8.22 \times 10{-}2$, an ultra-low effective material loss of 0.05 cm−1, and a very low confinement loss of $4.13{\times}10{-}5$ cm−1 at the frequency of 1 THz. Further investigation shows that about half of the total mode power confines into the air slots at 50% core porosity. The proposed fiber can be used for polarization maintaining applications in THz regime.
- A novel porous-core octagonal photonic crystal fiber (POPCF) for practical low loss terahertz (THz) wave guiding was suggested by Kaijagge. The POPCF with a porous core surrounded by an air-hole cladding shows a low material absorption loss of ∼0.07 cm−1, or one third of that for the bulk material absorption loss at the operating frequency ∼1 THz. In addition, the confinement loss, bending loss, and effective modal area properties of the POPCF are also reported and demonstrated to be relatively low. The proposed POPCF has potential applications for efficient transmission of broadband THz radiation.
- A photonic crystal fiber having ultralow material loss and near-zero dispersion at the telecom window which is suitable for THz wave guidance was proposed by Imran Hasan. The finite element method with perfectly matched layer circular boundary is used to investigate the guiding properties. The numerical results show that ultra-low material absorption loss of 0.056 cm−1 at 1.0 THz and nearly zero flattened dispersion of ±0.18 ps/THz/cm can be obtained from the proposed fiber in the wavelength range of 1.0–1.8 THz.
- This letter reports a photonic crystal fiber having ultralow material loss and near zero dispersion at the telecom window which is suitable for THz wave guidance. The finite element method with perfectly matched layer circular boundary is used to investigate the guiding properties. The numerical results show that ultra-low material absorption loss of 0.056 cm^{-1} at 1.0 THz and nearly zero flattened dispersion of ±0.18 ps/THz/cm can be obtained from the proposed fiber in the wavelength range of 1.0–1.8 THz.

- A new type of dielectric 1Hz waveguide, which evolved from a recent approach from the field of integrated optics, is presented with theoretical and experimental results. Due to the continuity of electric flux density at a dielectric interface, the THz wave is predominantly confined in the virtually lossless low index air core of a high-index dielectric waveguide. Attenuation, dispersion, field enhancement and field confinement properties of the waveguide are discussed and compared to those of other THz waveguide approaches.

CHAPTER 4
OUR PLATFORM: COMSOL MULTIPHYSICS VERSION 4.3B

4.1 Creating A New Model

We set up a model guided by the Model Wizard or start from a Blank Model.

4.1.1 Creating A Model Guided by The Model Wizard

The Model Wizard will guide you in setting up the space dimension, physics, and study type in a few steps:

1. Start by selecting the space dimension for your model component: 3D, 2D Axisymmetric, 2D, 1D Axisymmetric, or 0D.
2. Now, we add one or more physics interfaces. These are organized in a number of Physics branches in order to make them easy to locate. These branches do not directly correspond to products. When products are added to your COMSOL Multiphysics installation, one or more branches will be populated with additional physics interfaces.
3. We select the Study type that represents the solver or set of solvers that will be used for the computation. Finally, click Done. The desktop is now displayed with the model tree configured according to the choices you made in the Model Wizard.

4.1.2Creating A Blank Model

The Blank Model option will open the COMSOL Desktop interface without any Component or Study. You can right-click the model tree to add a Component of a certain space dimension, physics interface, or Study.

4.2 Parameters, Variables and Scope

4.2.1 Global Parameters

Global parameters are user-defined constant scalars that are usable throughout the model. That is to say, they are “global” in nature. Important uses are:

• Parameterizing geometric dimensions.

• Specifying mesh element sizes.

• Defining parametric sweeps (simulations that are repeated for a variety of different values of a parameter such as a frequency or load).

A global parameter expression can contain numbers, global parameters, built-in constants, built-in functions with global parameter expressions as arguments, and unary and binary operators. For a list of available operators, Language Elements and
Reserved Names”. Because these expressions are evaluated before a simulation begins, global parameters may not depend on the time variable t. Likewise, they may not depend on spatial variables like x, y, or z, nor on the dependent variables for which your equations are solving. It is important to know that the names of parameters are case sensitive. You define global parameters in the Parameters node in the model tree under Global Definitions.

4.2.2 Geometry

This tutorial uses a geometry that was previously created.
File Locations
The location of the application library that contains the file used in this exercise varies based on the software installation and operating system. In Windows, the file path will be similar to:

C:\Program Files\COMSOL\COMSOL52a\Multiphysics\applications.

1. In the Model Builder window, under Component 1, right-click Geometry 1 and select Import. As an alternative, you can use the ribbon and click Import from the Geometry tab.
2. In the Settings window for Import, from the Source list, select COMSOL

   Multiphysics file.

3. Click Browse and locate the file wrench.mphbin in the application library folder of the COMSOL installation folder. Its default location in Windows is:

C:\ProgramFiles\COMSOL\COMSOL52a\Multiphysics\applications\COMSOL_Multiphys ics\ Structural_Mechanics\wrench.mphbin

Double-click to add or click Open.

4.2.3 Materials

The Materials node stores the material properties for all physics and all domains in a Component node. Use the same generic steel material for both the bolt and tool. Here is how to choose it in the Model Builder.

1. Open the Add Materials window. You can open the Add Materials window in either of these two ways:

-Right-click Component 1 > Materials in the Model Builder and select Add Material

- From the ribbon, select the Home tab and then click Add Material.

2. In the Add Material window, click to expand the Built-In folder. Scroll down to find Structural steel, right-click, and select Add to Component 1.

3. Examine the Material Contents section in the Settings window for Material to see the properties that are available. Properties with green check marks are used by the physics in the simulation.
4. Close the Add Material window.

4.3 Selecting Boundaries and Other Geometric Entities

When a boundary is unselected, its color is typically gray, the exception being when you use the material Appearance setting available in Materials; To select a boundary, first hover over it. This highlights the boundary in red, assuming the boundary was previously unselected. Now, click to select the boundary by using the left mouse button. The boundary now turns blue. Its boundary number will appear in the Selection list in the Settings window of the corresponding boundary condition. Once a boundary is selected and you hover over it again, the boundary turns green. If you click a boundary highlighted in green, the boundary is deselected and now turns gray again.

The same technique for selecting and deselecting is applicable to geometry objects, domains, boundaries, edges, and points.

Mesh

The mesh settings determine the resolution of the finite element mesh used to discretize the model. The finite element method divides the model into small elements of geometrically simple shapes, in this case tetrahedrons. In each tetrahedron, a set of polynomial functions is used to approximate the structural displacement field — how much the object deforms in each of the three coordinate directions.

In this example, because the geometry contains small edges and faces, you will define a slightly finer mesh than the default setting suggests. This will better resolve the variations of the stress field and give a more accurate result. Refining the mesh size to improve computational accuracy always involves some sacrifice in speed and typically requires increased memory usage.

Study

In the beginning of setting up the model, you selected a Stationary study, which implies that a stationary solver will be used. For this to be applicable, the assumption is that the load, deformation, and stress do not vary in time. To start the solver:

Right-click Study 1 and select Compute (or press F8). After a few seconds of computation time, the default plot is displayed in the Graphics window. You can find other useful information about the computation in the Messages and Log windows; Click the Messages and Log tabs under the Graphics window to see the kind of information available to you. The Messages window can also be opened from the Windows drop-down list in the Home tab of the ribbon.

Results:

The von Mises stress is displayed in the Graphics window in a default Surface plot with the displacement visualized using a Deformation subnode. Change the default unit (N/m2) to the more suitable MPa as shown in the following steps.

CHAPTER 5
FACTORS AND LOSSES IN OPTICAL FIBER

5.1 Single Mode Fiber

In fiber-optic communication, a single-mode optical fiber (SMF) is an optical fiber designed to carry light only directly down the fiber - the transverse mode. Modes are the possible solutions of the Helmholtz equation for waves, which is obtained by combining Maxwell's equations and the boundary conditions. These modes define the way the wave travels through space, i.e. how the wave is distributed in space. Waves can have the same mode but have different frequencies. This is the case in single-mode fibers, where we can have waves with different frequencies, but of the same mode, which means that they are distributed in space in the same way, and that gives us a single ray of light. Although the ray travels parallel to the length of the fiber, it is often called transverse mode since its electromagnetic vibrations occur perpendicular (transverse) to the length of the fiber. The 2009 Nobel Prize in Physics was awarded to Charles K. Kao for his theoretical work on the single-mode optical fiber.

5.1.1 Characteristics

Like multi-mode optical fibers, single mode fibers do exhibit modal dispersion resulting from multiple spatial modes but with narrower modal dispersion. Single mode fibers are therefore better at retaining the fidelity of each light pulse over longer distances than multi-mode fibers. For these reasons, single-mode fibers can have a higher bandwidth than multi-mode fibers. Equipment for single mode fiber is more expensive than equipment for multi-mode optical fiber, but the single mode fiber itself is usually cheaper in bulk.

A typical single mode optical fiber has a core diameter between 8 and 10.5 μm and a cladding diameter of 125 μm. There are a number of special types of single-mode optical fiber which have been chemically or physically altered to give special properties, such as dispersion-fiber and nonzero dispersion-shifted fiber. Data rates are limited by polarization mode dispersion and chromatic dispersion. As of 2005, data rates of up to 10 gigabits per second were possible at

distances of over 80 km (50 mi) with commercially available transceivers (Xenpak). By using optical amplifiers and dispersion-compensating devices, state-of-the-art DWDM optical systems can span thousands of kilometers at 10 Gbit/s, and several hundred kilometers at 40 Gbit/s.

The lowest-order bounds mode is ascertained for the wavelength of interest by solving Maxwell's equations for the boundary conditions imposed by the fiber, which are determined by the core diameter and the refractive indices of the core and cladding. The solution of Maxwell's equations for the lowest order bound mode will permit a pair of orthogonally polarized fields in the fiber, and this is the usual case in a communication fiber.
In step-index guides, single-mode operation occurs when the normalized frequency, *V*, is less than or equal to 2.405. In practice, the orthogonal polarizations may not be associated with degenerate modes.

$$V = \frac{2\pi r f}{c}\sqrt{n_{co}^2 - n_{cl}^2} \leq 2.405 \ldots\ldots\ldots\ldots\ldots\ldots\ldots\ldots (5.1)$$

OS1 and OS2 are standard single-mode optical fiber used with wavelengths 1310 nm and 1550 nm (size 9/125 μm) with a maximum attenuation of 1 dB/km (OS1) and 0.4 dB/km(OS2). OS1 is defined in ISO/IEC 11801,[7] and OS2 is defined in ISO/IEC 24702.

5.2 Multi Mode Fiber

Multi-mode optical fiber is a type of optical_fiber mostly used for communication over short distances, such as within a building or on a campus. Typical multimode links have data rates of 10 Mbit/s to 10 Gbit/s over link lengths of up to 600 meters (2000 feet).

5.2.1 Applications

The equipment used for communications over multi-mode optical fiber is less expensive than that for single-mode optical fiber. Typical transmission speed and distance limits are 100 Mbit/s for distances up to 2 km (100BASE-FX), 1 Gbit/s up to 1000 m, and 10 Gbit/s up to 550 m.

Because of its high capacity and reliability, multi-mode optical fiber generally is used for backbone applications in buildings. An increasing number of users are taking the benefits of fiber closer to

the user by running fiber to the desktop or to the zone. Standards-compliant architectures such as Centralized Cabling and fiber to the telecom enclosure offer users the ability to leverage the distance capabilities of fiber by centralizing electronics in telecommunications rooms, rather than having active electronics on each floor.

5.2.2 Comparison with single-mode fiber

The main difference between multi-mode and single-mode optical fiber is that the former has much larger core diameter, typically 50–100 micrometers; much larger than the wavelength of the light carried in it. Because of the large core and also the possibility of large numerical aperture, multi-mode fiber has higher "light-gathering" capacity than single-mode fiber. In practical terms, the larger core size simplifies connections and also allows the use of lower-cost electronics such as light-emitting diodes (LEDs) and vertical-cavity surface-emitting lasers (VCSELs) which operate at the 850 nm and 1300 nm wavelength (single-mode fibers used in telecommunications typically operate at 1310 or 1550 nm). However, compared to single-mode fibers, the multi-mode fiber bandwidth–distance product limit is lower. Because multi-mode fiber has a larger core size than single-mode fiber, it supports more than one propagation mode; hence it is limited by modal dispersion, while single mode is not.

The LED light sources sometimes used with multi-mode fiber produce a range of wavelengths and these each propagate at different speeds. This chromatic dispersion is another limit to the useful length for multi-mode fiber optic cable. In contrast, the lasers used to drive single-mode fibers produce coherent light of a single wavelength. Due to the modal dispersion, multi-mode fiber has higher pulse spreading rates than single mode fiber, limiting multi-mode fiber’s information transmission capacity.
Single-mode fibers are often used in high-precision scientific research because restricting the light to only one propagation mode allows it to be focused to an intense, diffraction-limited spot.

Jacket color is sometimes used to distinguish multi-mode cables from single-mode ones. The standard TIA-598C recommends, for non-military applications, the use of a yellow jacket for single-mode fiber, and orange or aqua for multi-mode fiber, depending on type. Some vendors use violet to distinguish higher performance OM4 communications fiber from other types.

5.3 Material Absorption Loss

Absorption of signal is a serious loss mechanism in an optical fiber. Absorption occurs in optical fibers due to the presence of imperfections in the atomic structure of the fiber material, due to some basic inherent intrinsic material properties and due to some extrinsic material properties. Imperfections may appear in atomic structure due to oxygen deficiencies and missing of certain molecules. Diffusion of hydrogen molecules may also induce absorption. But the contribution from imperfections is relatively small in fiber optic absorption losses. Inherent intrinsic absorption is caused by basic fiber material properties. If a material is free from impurities and imperfections, then entire absorption is due to intrinsic absorption. Silica fibers possess very low intrinsic material absorption. Here absorption is caused by the vibration of silicon-oxygen bonds. The interaction between these bonds and the electromagnetic field of the optical signal is responsible for intrinsic absorption. Presence of impurities in the fiber material leads to extrinsic absorption. This is caused by the electronic transition of metal impurity ions from one energy level to another. Another reason for extrinsic absorption is the presence of hydroxyl ions in the fiber.

$$\alpha_{eff} = \sqrt{\frac{\varepsilon_0}{\mu_0}} \left(\frac{\int_{mat} n_{mat} |E|^2 \alpha_{mat} dA}{\int_{all} S_z dA} \right) \quad \text{.....(5.2)}$$

Where, ε_0 and μ_0 are considered to be the relative permittivity and permeability in vacuum respectively, n_{mat} is the refractive index of Topaz, α_{mat} is the bulk material absorption loss, $\boldsymbol{E}$ is the modal electric field and S_z is the z component of the pointing vector ($S_z = ½(\mathbf{E} \times \mathbf{H}^*).z$),where **E** and **H** are the electric and magnetic fields respectively.Fig.5 depicts the characteristics of EML as a function of core diameter with different core porosities. From where it is observed that, for the same porosity values there is a significant change of EML when the core diameter changes.

It is a loss mechanism related to the material composition and fabrication process of the fiber which results in the dissipation of some of the transmitted optical power as heat in waveguide. The absorption of light may be intrinsic (caused by one or more major components of glass) or extrinsic (caused by impurities within the glass).

5.4 Mode Power Propagation

The amount of useful power propagating through different regions of the fiber also known as core power fraction can be calculated by,

$$\eta' = \frac{\int_x \dot{S}_z dA}{\int_c S_z dA} \quad \text{.....(5.3)}$$

Where η' represents mode power fraction and X represents the area of interests. To design a standard PCF, it is necessary to pass most of the useful power through the core air holes. Higher D_{core} increases the core power fraction but this also increases the EML. On the other hand, as the D_{core} decreases EML also decreases but this also decreases the core power fraction. These are contradictory conditions and needs to select an optimum condition of higher core power fraction and lower EML. At different core porosities, the characteristics of core power fraction as a function of core diameter where it can be observed that amount of core power increases with the increase of core diameter.

5.5 Confinement Loss

PCFs are a new class of optical fibers, which has concerned fabulous attention in the last few years. PCFs are normally formed with silica having air holes positioned in the cladding region. PCFs have novel properties because the effective refractive index has burly wavelength dependence and huge design flexibility. PCFs main applications range from telecommunication field to metrology, spectroscopy, microscopy, medical diagnostics equipment, biology and sensing. There are several parameters to manipulate: pitch, air hole shape and diameter, refractive index of the glass, and type of lattice. PCFs structures can have hexagonal lattice or octagonal lattice or square lattice. By changing the lattices and lattice parameters like pitch, air hole diameter and changing rings in the cladding region, the properties of PCFs can also be changed.

Many experiments and investigations have been carried out using different analysis techniques and tools to understand the propagation properties of various PCFs. PCFs also known as micro-structured or holey fibers are made of the refractive index periodicity, with the arrangement of air holes around the core. Many rings around the core help to ensnare light well within the core minimizing the confinement loss. Based on structure, PCFs can be either solid core high-index

guiding fibers or hollow core low index guiding fibers. The index guiding PCFs guide light in a solid core by modified total internal reflection (M-TIR) like to the conventional optical fibers. Hollow core PCFs guide light by the photonic band gap (PBG) effect. Light is confined in the low-index core, as the distribution of energy levels in the structure makes the propagation in the cladding region impossible. In both cases, to attain the lowest amount loss, air holes should be continual to infinity which is unfeasible. So, modes leak in cladding and confinement loss is created. The confinement loss can be reduced by proper design of structure parameters in PCFs, and consequently, mode leakage to cladding is avoided. Already, many reports have been published about PCFs with low confinement loss. At 0.8 μm center wavelength the confinement loss is found 10-8dB/m, 10-6dB/m and 10-4 dB/m for 2 μm, 1.8 μm and 1.6 μm lattice pitches. Again at 1.55 μm center wavelength for three rings hexagonal PCFs the confinement loss is 10-3 dB/km but Ademgil and Huxha obtained this loss which was varied from 10-1to 10-5dB/m [10]. Also, at 1.3 μm center wavelength this confinement loss was found 10-8dB/km for circular ring PCFs.

Another important parameter to be considered for PCF design is confinement loss. It depends upon the core porosity and the number of air holes used in cladding. It can be calculated by taking the imaginary part of the complex refractive index. The confinement loss can be calculated by,

$$L_c = 8.686\left(\frac{2\pi f}{c}\right) Im(n_{eff})\left(\frac{dB}{m}\right) \ldots\ldots\ldots\ldots\ldots\ldots\ldots\ldots (5.4)$$

Where, *f* is the frequency of the guiding light, *c* is speed of light in vacuum and Im*(*n_{eff}*)* symbolizes the imaginary part of the refractive index. The confinement loss as a function of frequency where it is observed that as the frequency increases, the confinement loss scaled down.

5.6 Dispersion

In optics, dispersion is the phenomenon in which the phase velocity of a wave depends on its frequency. Media having this common property may be termed dispersive media. Sometimes the term chromatic dispersion is used for specificity. Although the term is used in the field of optics to describe light and other electromagnetic waves, dispersion in the same sense can apply to any sort of wave motion such as acoustic dispersion in the case of sound and seismic waves, in gravity waves (ocean waves), and for telecommunication signals propagating along transmission lines (such as coaxial cable) or optical fiber.

In optics, one important and familiar consequence of dispersion is the change in the angle of refraction of different colors of light, as seen in the spectrum produced by a dispersive prism and in chromatic aberration of lenses. Design of compound achromatic lenses, in which chromatic aberration is largely cancelled, uses a quantification of a glass's dispersion given by its Abbe number V, where lower Abbe numbers correspond to greater dispersion over the visible spectrum. In some applications such as telecommunications, the absolute phase of a wave is often not important but only the propagation of wave packets or "pulses"; in that case one is interested only in variations of group velocity with frequency, so-called group-velocity dispersion (GVD).

5.6.1 Material and waveguide dispersion

Most often, chromatic dispersion refers to bulk material dispersion, that is, the change in refractive index with optical frequency. However, in a waveguide there is also the phenomenon of waveguide dispersion, in which case a wave's phase velocity in a structure depends on its frequency simply due to the structure's geometry. More generally, "waveguide" dispersion can occur for waves propagating through any inhomogeneous structure (e.g., a photonic crystal), whether or not the waves are confined to some region. In a waveguide, both types of dispersion will generally be present, although they are not strictly additive. For example, in fiber optics the material and waveguide dispersion can effectively cancel each other out to produce a Zero dispersion important for fast Fiber-optic communication.

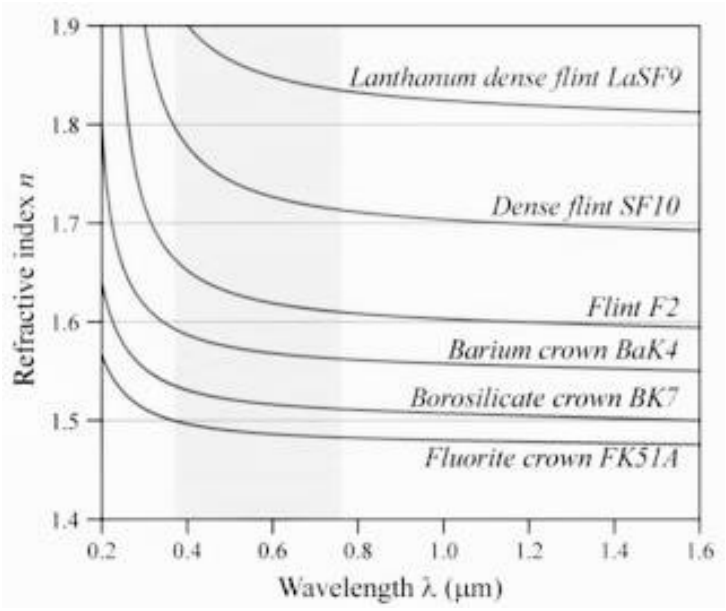

Fig 5.1 Material dispersion in optics

The variation of refractive index vs. vacuum wavelength for various glasses. The wavelengths of visible light are shaded in red.

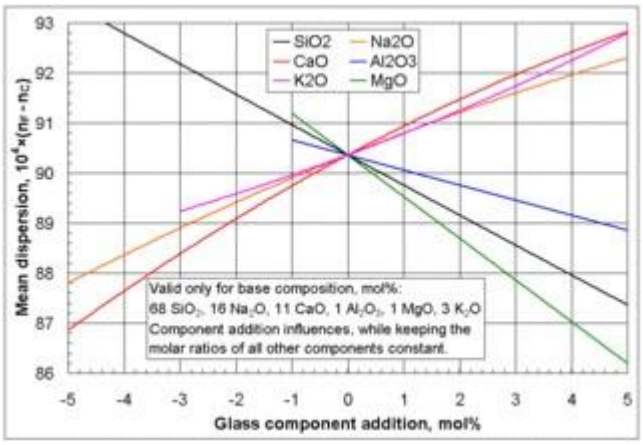

Fig 5.2 Mean dispersion in terms of mole

Influences of selected glass component additions on the mean dispersion of a specific base glass (n_F valid for $\lambda = 486$ nm (blue), n_C valid for $\lambda = 656$ nm (red).

Material dispersion can be a desirable or undesirable effect in optical applications. The dispersion of light by glass prisms is used to construct spectrometers and Spectro radiometers. Holographic gratings are also used, as they allow more accurate discrimination of wavelengths. However, in lenses, dispersion causes chromatic aberration, an undesired effect that may degrade images in microscopes, telescopes and photographic objectives.

In general, the refractive index is some function of the frequency f of the light, thus n = n(f), or alternatively, with respect to the wave's wavelength n = n(λ). The wavelength dependence of a material's refractive index is usually quantified by its Abbe number or its coefficients in an empirical formula such as the Cauchy or Sellmeier equations.

Because of the Kramers–Kronig relations, the wavelength dependence of the real part of the refractive index is related to the material absorption, described by the imaginary part of the refractive index (also called the extinction coefficient). In particular, for nonmagnetic materials ($\mu = \mu_0$), the susceptibility χ that appears in the Kramers–Kronig relations is the electric susceptibility $\chi_e = n^2 - 1$.

The most commonly seen consequence of dispersion in optics is the separation of white light into a color spectrum by a prism. From Snell's law it can be seen that the angle of refraction of light in a prism depends on the refractive index of the prism material. Since that refractive index varies with wavelength, it follows that the angle that the light is refracted by will also vary with wavelength, causing an angular separation of the colors known as angular dispersion.

In this case, the medium is said to have normal dispersion. Whereas, if the index increases with increasing wavelength (which is typically the case for X-rays, the medium is said to have anomalous dispersion.

At the interface of such a material with air or vacuum (index of ~1), Snell's law predicts that light incident at an angle θ to the normal will be refracted at an angle $\arcsin(\sin \theta/n)$. Thus, blue light, with a higher refractive index, will be bent more strongly than red light, resulting in the well-known rainbow pattern.

5.6.2 Group Velocity Dispersion

Another consequence of dispersion manifests itself as a temporal effect. The formula $v = c/n$ calculates the phase velocity of a wave; this is the velocity at which the phase of any one frequency component of the wave will propagate. This is not the same as the group velocity of the wave, that is the rate at which changes in amplitude (known as the envelope of the wave) will propagate. For a homogeneous medium, the group velocity v_g is related to the phase velocity v by (here λ is the wavelength in vacuum, not in the medium):

The group velocity v_g is often thought of as the velocity at which energy or information is conveyed along the wave. In most cases this is true, and the group velocity can be thought of as the signal velocity of the waveform. In some unusual circumstances, called cases of anomalous dispersion, the rate of change of the index of refraction with respect to the wavelength changes sign (becoming negative), in which case it is possible for the group velocity to exceed the speed of light ($v_g > c$). Anomalous dispersion occurs, for instance, where the wavelength of the light is close to an absorption resonance of the medium. When the dispersion is anomalous, however, group velocity is no longer an indicator of signal velocity. Instead, a signal travels at the speed of the wavefront, which is c irrespective of the index of refraction. Recently, it has become possible to create gases in which the group velocity is not only larger than the speed of light, but even negative. In these

cases, a pulse can appear to exit a medium before it enters. Even in these cases, however, a signal travels at, or less than, the speed of light, as demonstrated by Stenner, et al.

The group velocity itself is usually a function of the wave's frequency. This results in group velocity dispersion (GVD), which causes a short pulse of light to spread in time as a result of different frequency components of the pulse travelling at different velocities. GVD is often quantified as the group delay dispersion parameter (again, this formula is for a uniform medium only).

If D is less than zero, the medium is said to have positive dispersion. If D is greater than zero, the medium has negative dispersion. If a light pulse is propagated through a normally dispersive medium, the result is the higher frequency components travel slower than the lower frequency components. The pulse therefore becomes positively chirped, or up-chirped, increasing in frequency with time. Conversely, if a pulse travels through an anomalously dispersive medium, high frequency components travel faster than the lower ones, and the pulse becomes negatively chirped, or down-chirped, decreasing in frequency with time.

The result of GVD, whether negative or positive, is ultimately temporal spreading of the pulse. This makes dispersion management extremely important in optical communications systems based on optical fiber, since if dispersion is too high, a group of pulses representing a bit-stream will spread in time and merge, rendering the bitstream unintelligible. This limits the length of fiber that a signal can be sent down without regeneration. One possible answer to this problem is to send signals down the optical fiber at a wavelength where the GVD is zero (e.g., around 1.3–1.5 μm in silicafibres), so pulses at this wavelength suffer minimal spreading from dispersion. In practice, however, this approach causes more problems than it solves because zero GVD unacceptably amplifies other nonlinear effects (such as four wave mixing). Another possible option is to use soliton pulses in the regime of anomalous dispersion, a form of optical pulse which uses a nonlinear optical effect to self-maintain its shape. Solitons have the practical problem, however, that they require a certain power level to be maintained in the pulse for the nonlinear effect to be of the correct strength. Instead, the solution that is currently used in practice is to perform dispersion compensation, typically by matching the fiber with another fiber of opposite-sign dispersion so that the dispersion effects cancel; such compensation is ultimately limited by nonlinear effects such as self-phase modulation, which interact with dispersion to make it very difficult to undo.

Dispersion control is also important in lasers that produce short pulses. The overall dispersion of the optical resonator is a major factor in determining the duration of the pulses emitted by the laser. A pair of prisms can be arranged to produce net negative dispersion, which can be used to balance the usually positive dispersion of the laser medium. Diffraction gratings can also be used to produce dispersive effects; these are often used in high-power laser amplifier systems. Recently, an alternative to prisms and gratings has been developed: chirped mirrors. These dielectric mirrors are coated so that different wavelengths have different penetration lengths, and therefore different group delays. The coating layers can be tailored to achieve a net negative dispersion.

5.6.3 Dispersion in waveguides

Waveguides are highly dispersive due to their geometry (rather than just to their material composition). Optical fibers are a sort of waveguide for optical frequencies (light) widely used in modern telecommunications systems. The rate at which data can be transported on a single fiber is limited by pulse broadening due to chromatic dispersion among other phenomena.
In general, for a waveguide mode with an angular frequency ω(β) at a propagation constantβ (so that the electromagnetic fields in the propagation direction z oscillate proportional to $e^{i(\beta z-\omega t)}$), the group-velocity dispersion parameter D is defined as:

$$\beta_2 = \frac{2}{c}\frac{dn_{eff}}{d\omega} + \frac{\omega}{c}\frac{d^2 n_{eff}}{d\omega^2} \quad \text{.....(5.5)}$$

Where, $\lambda = 2\pi c/\omega$ is the vacuum wavelength and $v_g = d\omega/d\beta$ is the group velocity. This formula generalizes the one in the previous section for homogeneous media, and includes both waveguide dispersion and material dispersion. The reason for defining the dispersion in this way is that |D| is the (asymptotic) temporal pulse spreading Δt per unit bandwidth Δλ per unit distance travelled, commonly reported in ps / nm km for optical fibers.

In the case of multi-mode optical fibers, so-called modal dispersion will also lead to pulse broadening. Even in single-mode fibers, pulse broadening can occur as a result of polarization mode dispersion (since there are still two polarization modes). These are not examples of chromatic dispersion as they are not dependent on the wavelength or bandwidth of the pulses propagated.

5.7 Effective Area

The effective area (A_{eff}) of the proposed fiber is also discussed, which can be calculated by [33]

$$A_{eff} = \frac{[\int I(r) r dr]^2}{[\int I^2(r) r dr]^2} \ldots\ldots\ldots\ldots\ldots\ldots\ldots\ldots (5.6)$$

Where; $I(r) = |E_t|^2$ is defined as the transverse electric field intensity distribution in the cross section of the fiber. The A_{eff} as a function of frequency, from where it is observed that as the frequency increases from 0.9 THz the A_{eff} decreases. It is because of more light spread for f>1 THz. It is also observed that at operating parameters, the calculated A_{eff} is very much comparable.

CHAPTER 6
PREVIOUS WORK ON SENSITIVITY APPLICATION

To design PCF COMSOL Multi-Physics is used widely. It can be interface with MATLAB for programming & plotting.

6.1 Overview of This Design

A highly sensitive porous core-photonic crystal fiber (PC-PCF) was designed and analyzed for remote detection of chemical analytes in terahertz frequency range. The PCPCF was modelled using rectangular structured air holes in the core with Kagome structured cladding. The full vectorial Finite Element Method (FEM) had been used to tune the geometrical parameters also to characterize the fiber. Simulation results demonstrate a high Relative Chemical Sensitivity with Lower Confinement Loss for different analytes. Moreover, the PCF shows low Dispersion Variation, high Modal Effective Area, high Birefringence and high Numerical Aperture (NA). The practical implementation of the fiber is feasible with the present fabrication techniques.

6.2 Design Methodology Followed

Rectangular structured air holes inside the core with kagome cladding was proposed. The rectangular structure is responsible to increase the birefringence and compact geometry of the PC-PCF is responsible for high sensitivity as well as flat dispersion characteristics. Here kagome structure in the cladding is chosen.

In Fig. 6.1, D_{core} shows the diameter of the core, the centre to centre distance between two air holes in the core region is denoted by P_c which is also known as core pitch, w indicates the core air hole

width, and L, L_1, L_2, L_3, and L_4 indicates the lengths of the core air holes which are 372 μm, 332 μm, 288 μm, 244 μm, and 198 μm respectively.

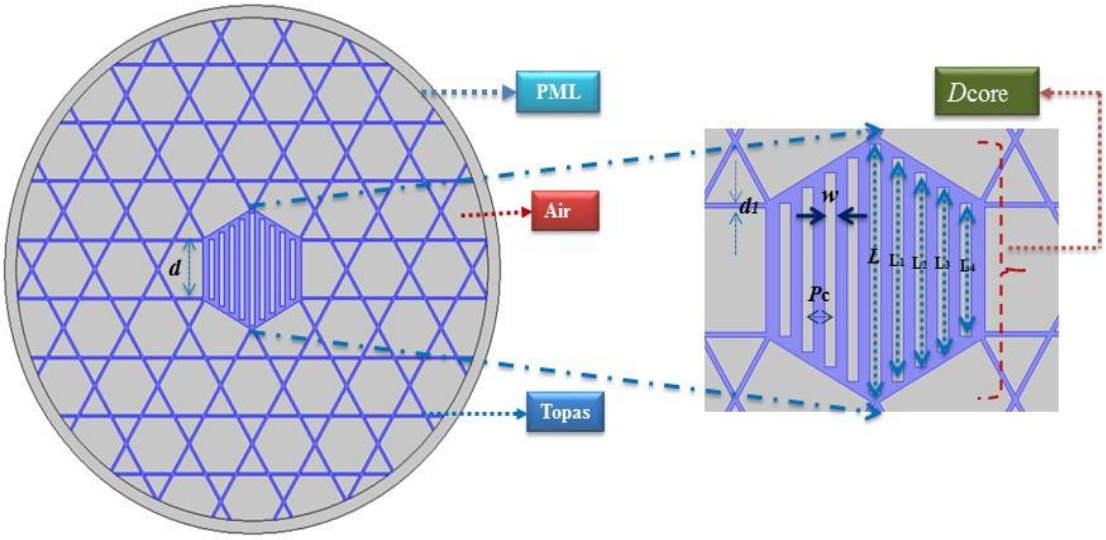

Fig. 6.1: Cross section of the terahertz PC-PCF sensor with its enlarged version of the core.

The optimum values of D_{core}, P_c and w are 360 μm, 38.38 μm and 32.32 μm respectively. For the kagome region, the distance between parallel struts and the strut width and are defined as d and d_1. Their optimum diameters are 195.38 μm and 4 μm respectively.

6.3 Simulations

6.3.1 Mode Power Distribution

The intensity of light interaction with the chemicals (water, ethanol & benzene) is shown in Fig. 6.2.

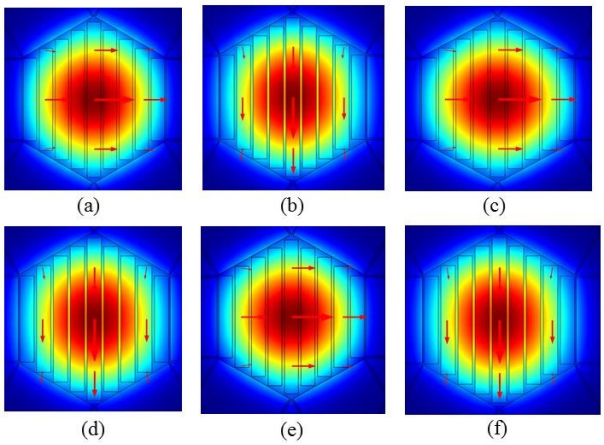

Fig. 6.2: Mode power distribution of the proposed PC-PCF for (a) water, *x*-pol (b) water, *y*-pol (c) ethanol, *x*-pol (d) ethanol, *y*-pol (e) benzene, *x*-pol (f) benzene, *y*-pol

6.3.2 Relative Sensitivity

The relative sensitivity of the proposed PC-PCF as a function of frequency and in the *x*-polarization mode with a rectangular hole width of 32.5 μm is shown in Fig. 8.3. The length of the slotted holes in the core region were kept fixed for all numerical simulations.

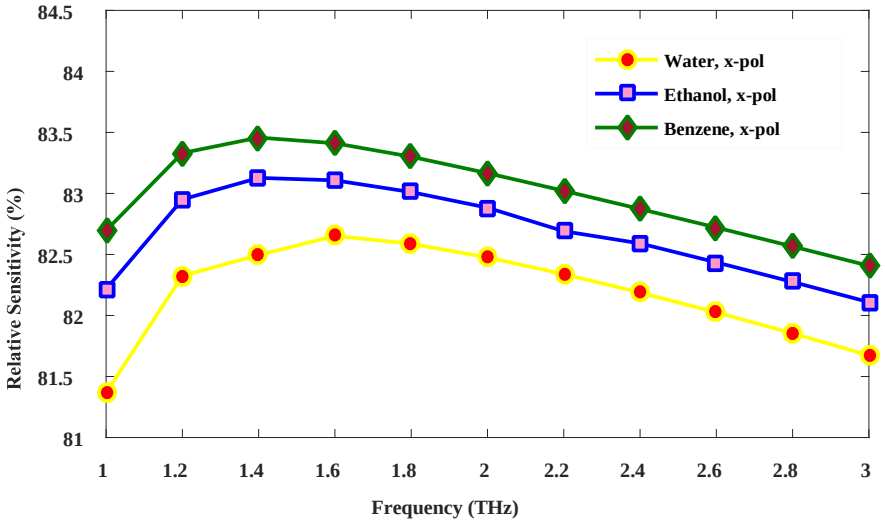

Fig. 6.3: Relative Sensitivity of water, ethanol & benzene as a function of frequency at *x*-polarization mode.

Three different analytes were used to test the sensitivity of the proposed chemical sensor. The analytes are water (n = 1.33), ethanol (n = 1.356), and benzene (n = 1.36).

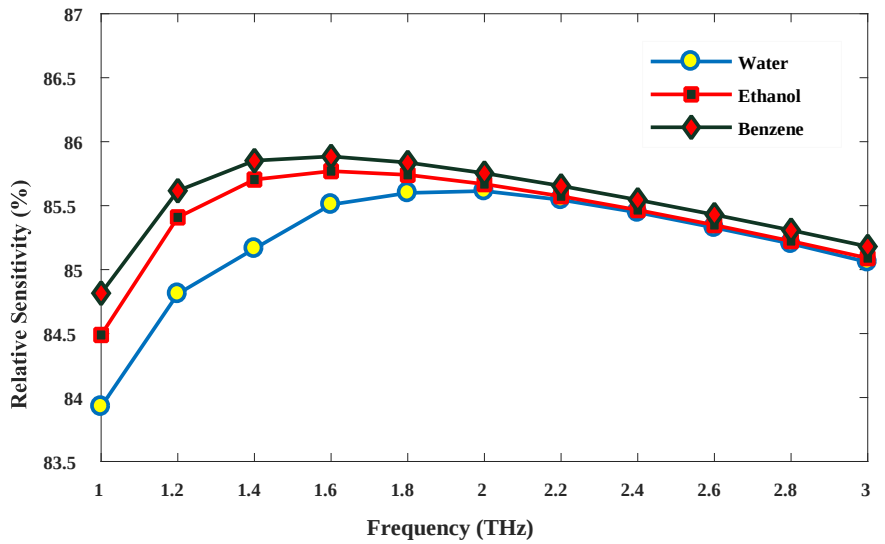

Fig. 6.4: Relative Sensitivity of water, ethanol benzene as a function of frequency at *y*-polarization mode.

At 1.6 THz, 32.5 μm slotted hole width and *x*-polarization mode the relative sensitivity for water, ethanol and benzene are 83.4%, 83.1%, and 82.6% respectively. The relative sensitivity obtained for the *y* polarization for water, ethanol and benzene are 85.6%, 85.7%, and 85.9% respectively.

Now, considering the practical realization of the proposed sensor, publisher tested the fibers ability

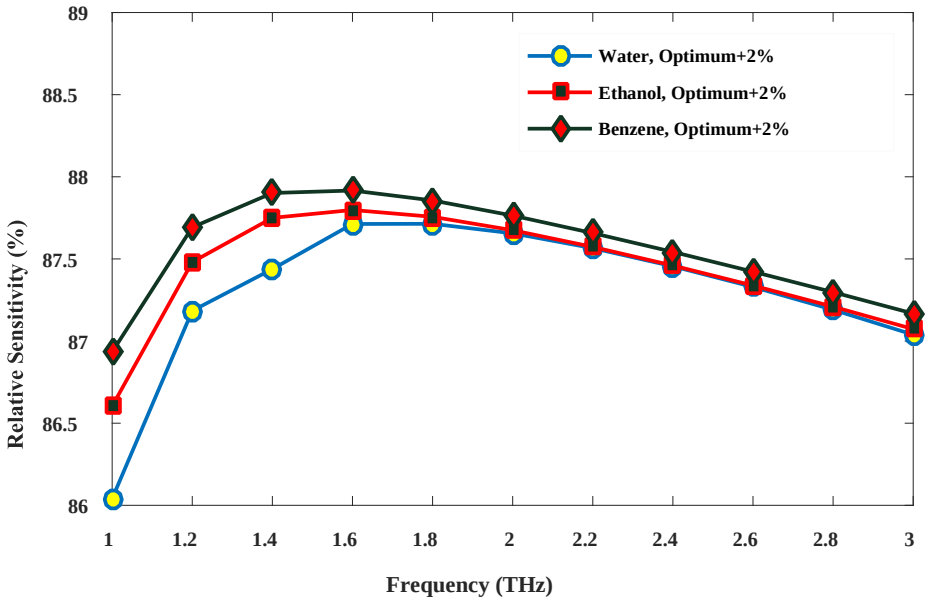

Fig. 6.5: Relative Sensitivity of water, ethanol & benzene as a function of frequency with 2% more than optimum design parameters.

to sense chemical by varying the core hole width to ±2% because during fabrication ±2% structural variation of the PC-PCF can happen. By increasing the slotted holes, the sensitivity becomes slightly higher than obtained for optimum value which is shown in Fig. 6.5. The relative sensitivity obtained in this case are 87.6%, 87.7%, and 87.9% respectively for 2% increasing of core hole width and 83.6%, 83.7%, and 83.8% for 2% reduction of core air hole width as shown in Fig. 6.6. So, considering Fig. 6.3, Fig. 6.4, Fig. 6.5, and Fig. 6.6 y-polarization mode is chosen, 1.6 THz frequency and 32.5 μm slotted hole diameter as optimum for this PC-PCF.

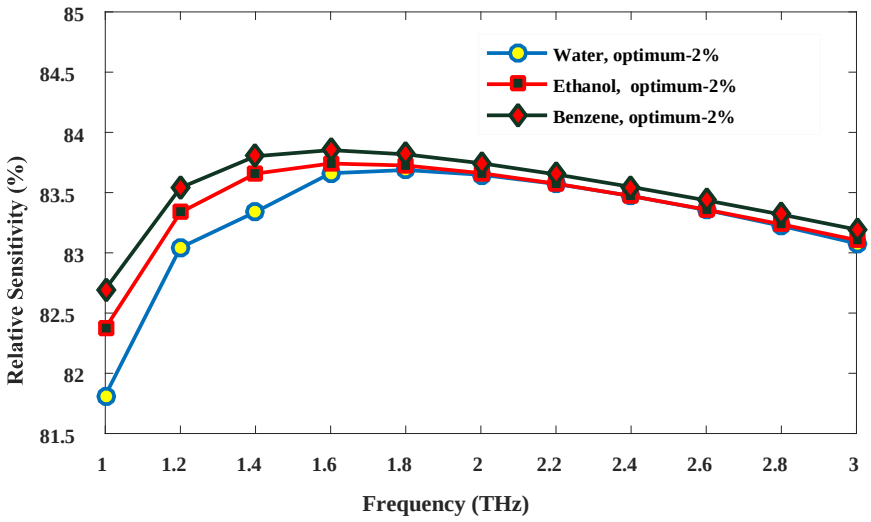

Fig. 6.6: Relative Sensitivity of chemicals as a function of frequency with 2% less than optimum design parameters

At optimal design parameters the obtained birefringence's were 0.006432414, 0.004987792, and 0.004331584 respectively for (n = 1.33), (n = 1.356), and (n = 1.36).

6.3.3 Confinement Loss

The obtained confinement loss for water, ethanol and benzene were 4.5649×10^{-9} cm^{-1}, 1.6771×10^{-9} cm^{-1}, and 1.0244×10^{-9} cm^{-1} respectively.

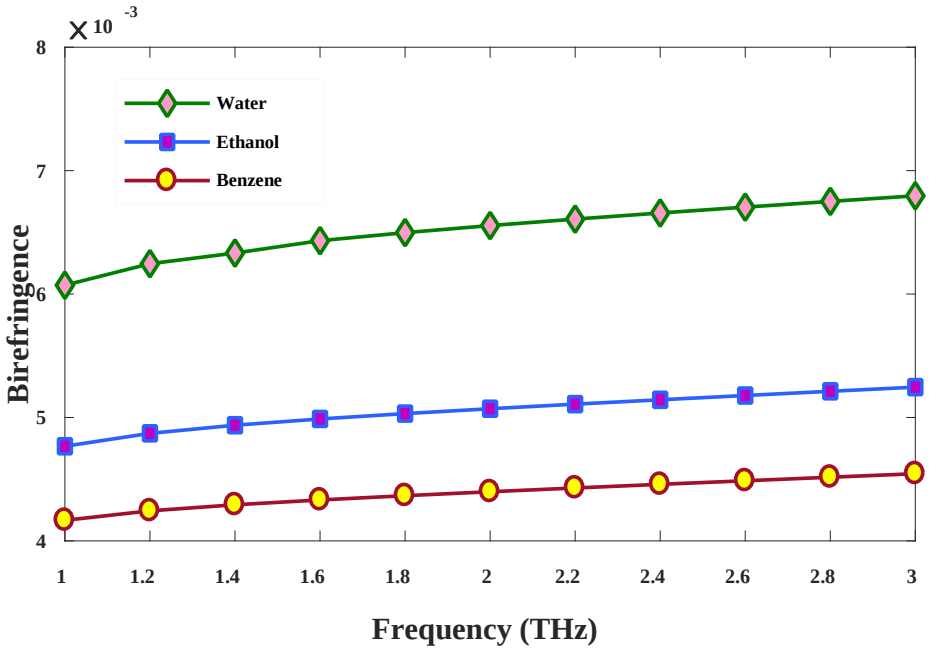

Fig. 6.7: Relative Sensitivity of water, ethanol benzene as a function of frequency with 2% less than optimum design parameters

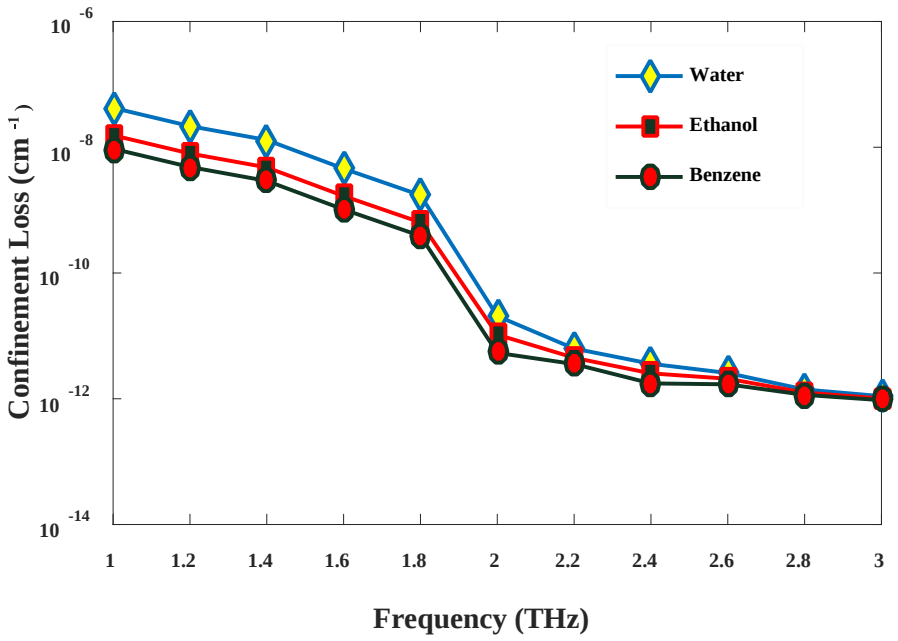

Fig. 6.8: Confinement loss of water, ethanol benzene as a function of frequency at optimum design parameters

6.3.4 Dispersion

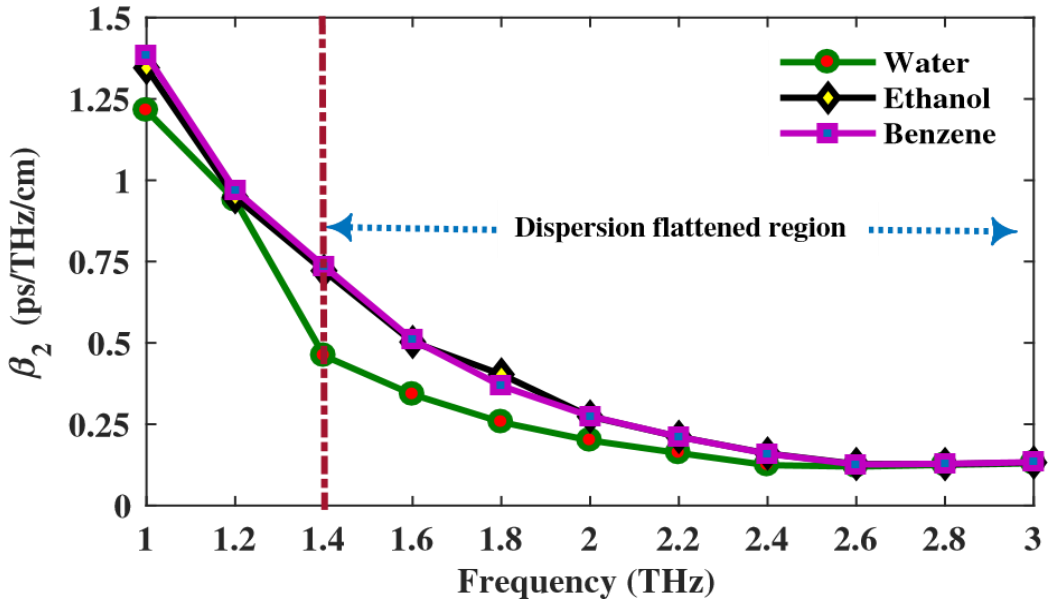

Fig. 6.9: Dispersion as a function of frequency at optimum design parameters

The feature of dispersion of the proposed sensor for different chemicals was shown in Fig. 6.9. At optimal design parameters it can be observed that, this fiber showed a dispersion flatness property within a broad-spectrum range of 1.4 THz to 3 THz. The obtained dispersion flatness of water,

ethanol and benzene were 0.325 ± 0.125 ps/THz/cm, 0.465 ± 0.265 ps/THz/cm, and 0.48 ± 0.27 ps/THz/cm respectively.

6.3.5 Effective Area

The behavior of effective area as a function of frequency is shown in Fig. 8.10. For water, ethanol and benzene the obtained effective areas are 71100 μm^2, 69800 μm^2, and 69300 μm^2 respectively.

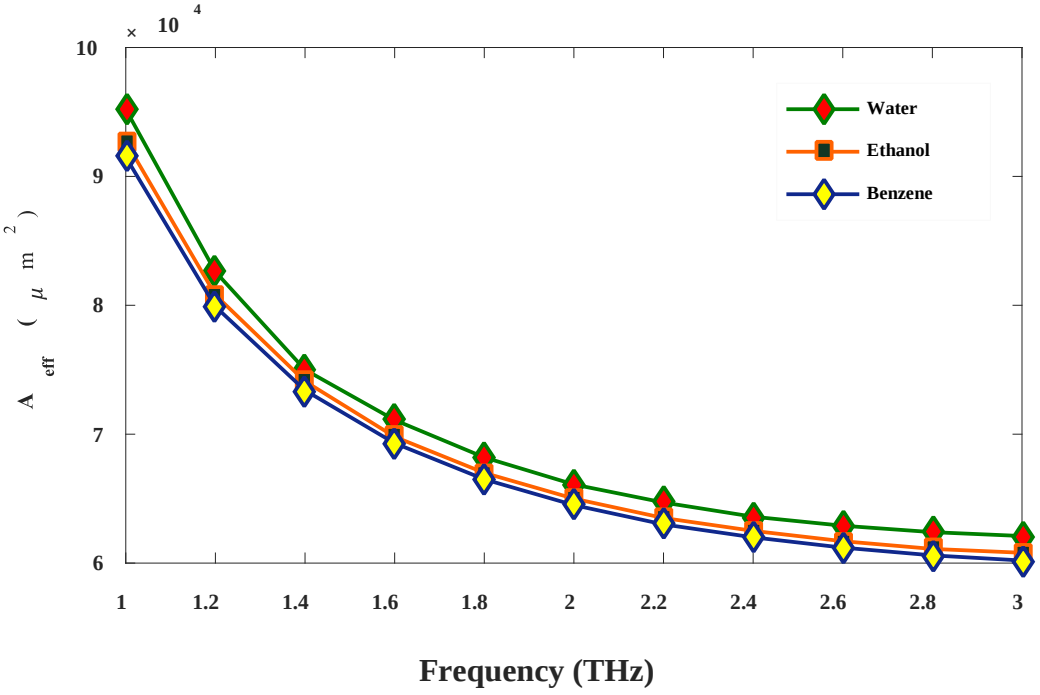

Fig. 6.10: Effective area as a function of frequency at optimum design parameters

6.3.6 Numerical Aperture

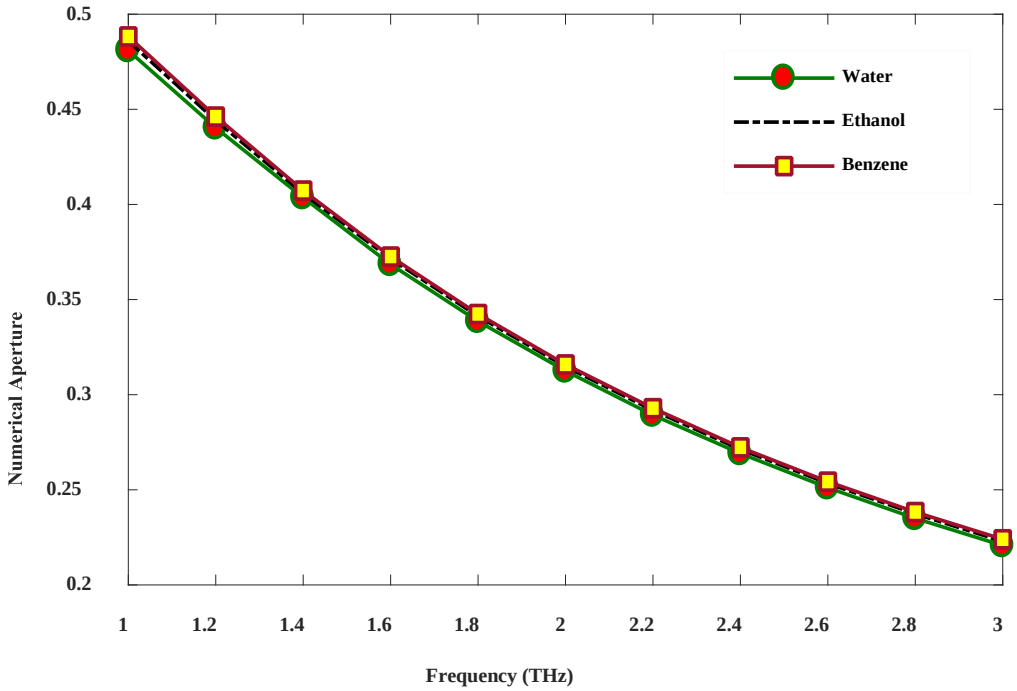

Fig. 6.11: Numerical Aperture as a function of frequency at optimum design parameters

The characteristics of Numerical Aperture with frequency variation and other optimal design parameters is shown in Fig. 6.11. It can be seen that numerical aperture decreases with frequency. A high value of NA of 0.4809, 0.4859 and 0.4883 is obtained at 1 THz frequency however as the main concern of the proposed PC-PCF is to increase the sensitivity so we choose 1.6 THz as optimum where the obtained NA is 0.3685, 0.3726, and 0.3715 for water, ethanol and benzene respectively.

CHAPTER 7
OUR PROPOSED DESIGN

7.1 Overview

A novel highly sensitive porous core-photonic crystal fiber (PC-PCF) has been designed and analyzed for remote detection of chemical analytes in terahertz frequency range. The PC-PCF has been modelled using rectangular structured air holes in the core with square structured cladding. The full vectorial finite element method (FEM) has been used to tune the geometrical parameters also to characterize the fiber. Simulation results demonstrate a high relative chemical sensitivity. Moreover, the PCF shows very low near zero dispersion variation, high modal effective area, high birefringence and high numerical aperture (NA). The practical implementation of the fiber is feasible with the present fabrication techniques. The optimized PCF with such attractive characteristic has commercial applications in remote chemical sensing as well as polarization preserving applications of terahertz waves.

In recent years, terahertz PCF has become a versatile approach for applications in sensing [38]-[42] time domain spectroscopy [43], biotechnology [43], analysis of RNA, DNA, and proteins in low frequency pulsation [44]-[47], intraoperative breast cancer and colon cancer [48]-[51], diagnosis of skin cancer [52], and the real-time detection of cancer vs. noncancer cells [49]. Terahertz is suitable than *x*-ray in operating room environment because it does not produce any ionizing radiation [49].

Moreover, terahertz frequency region bridges the gap between the microwave and the infra-red region in the electromagnetic frequency spectrum also being the transition region between electronics and photonics (as shown in Fig. 7.1) it attracts attention to scientific community to further research on it. But due to the insufficiency of suitable waveguide most of the terahertz system still largely dependent on air for its wave propagation. Dependent on air for wave propagation experiences path loss, large absorption loss and difficulties to integration with other components [54].

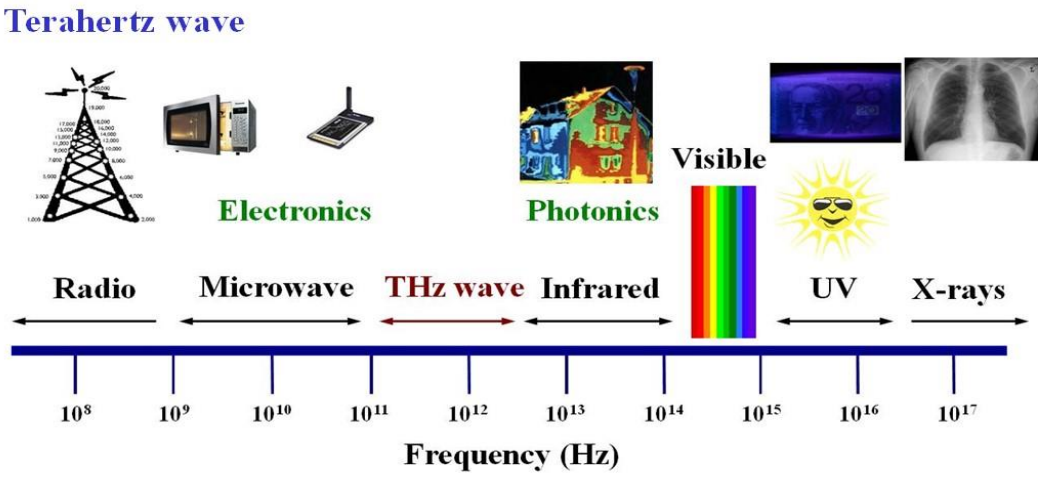

Fig. 7.1: Electromagnetic frequency spectrum.

To overcome the difficulties, we choose porous core PCF in designing the sensor because it provides a diversity of improved and new optical properties than that of conventional fibers. The biggest advantage is that, by varying the air hole size and position in both the core and cladding region in the transmission spectrum of the fiber, the birefringence, dispersion, effective area, NA, air filling fraction (AFF), frequency, can be modified to achieve values that are not gettable from conventional optical fibers. Moreover, in a PC-PCF the existence of air holes raises the option to pass electromagnetic waves through the air. PCF also advances its possibility to apply it into sensing application.

It is possible to replace the air from the air holes by chemical/gases and it might create a strong interaction between the light and sample which is nearly impossible to achieve using conventional optical fibers [53]. Moreover, PCF based sensors are advantageous because of its low cost, high sensitivity, robustness, small in size, flexibility that provides efficient solution of different industries. Moreover, PCFs sensor can operate in hostile environmental conditions such as at dynamic electromagnetic fields, high temperatures, noisy, high voltage, chemically destroying, and radiation of nuclear power [53].

There are a number of PC-PCFs [54]-[59] designed for low loss and polarization maintaining applications of terahertz waves but none of them extracts the application of PCF for sensing purposes in the terahertz frequency range.

From the last few decades, researchers proposed a number of research work for investigating several analytes (liquids/gases) [60]-[62]. At the beginning, researchers demonstrated that micro-structured PCFs [61], [64] can be a suitable candidate for sensing solutions. They investigated the optical and geometrical properties of micro-structured fibers for sensing applications.

In 2008, for remote investigation of chemical solutions a laser-terahertz emission system was proposed. They observed that amplitude of the sensitivity increases with the increasing of pH value of chemical [63]. However, the system requires extra biasing voltage to increase the sensitivity [63].

A PCF based intensity modulated temperature sensor filled with ethanol has been demonstrated by Yu *et. al.* [65]. A new type of chemical sensor based on hydrolysed polymerized crystalline colloidal (HPCC) array was proposed by Lee *et. al* [66]. The designed sensor was able to detect the P^H and ionic strength of a chemical.

In 2014, researchers proposed [67] an octagonal PCF and comprises with hexagonal PCF for sensing application. They found that in optical wavelength octagonal PCF provides higher sensitivity and lower losses than hexagonal PCF.

In 2015, Ademgil *et al.* [69] proposed an elliptical air hole based PC-PCF for chemical sensing applications in the optical wavelength. They obtained a relative sensitivity of 23.75% for benzene and further lower for ethanol and water. Moreover, their obtained confinement loss was also high and birefringence was low. In addition, they did not calculate the dispersion variation and NA of their proposed sensor.

Later, for chemical sensing application of PCF a hybrid core PCF was proposed [70]. They used elliptical shaped air holes to obtain a relative sensitivity of 49.17% with a confinement loss of 2.75×10^{-10} dBm^{-1}. They also obtained a low birefringence of 0.0018.

Later, for improvement in sensitivity and reduction in loss Arif *et. al.* [69] proposed a hexagonal PCF. The investigated that, by increasing the diameter of the first ring of cladding higher relative sensitivity can be achieved. Doing such they obtained a relative sensitivity of 59% with low confinement loss of the order of 10^{-11} dBm^{-1} for liquid sensing application.

Later, an octagonal PCF for alcohol sensing in the O+E+S+C+L+U transmission band was proposed by Paul *et. al.* [70]. By imposing silica as the background material, they obtained a relative sensitivity of 69.09% for benzene and lower confinement loss of 4.99×10^{-9} dBm^{-1}. Recently, a numerical investigation of a micro-array core based circular PCF was proposed for chemical sensing application [71]. They illustrate that increasing the air hole diameter of the outermost rings reduces the confinement loss. After simulating the PCF using FEM, they obtained a relative sensitivity of 29.25% for ethanol with a confinement loss of 7.68×10^{-7} cm^{-1}. However, they neglect to mention the characteristics of birefringence of their proposed PCF even they used asymmetrical air holes inside the core.

In 2017, Paul *et. al.* [72] proposed a folded cladded based PCF with a relative sensitivity of 65.18% and confinement loss of 2.07×10^{-5} dBm^{-1}. In it worthwhile to mention that, the sensors proposed in Ref. [67]-[72] used silica as the background material. Moreover, they all characterize their designed sensor into optical length. Investigating their [67]-[72] obtained results it is found that the obtained relative sensitivity is not up to the mark. So, we found there is a large scope of development in PCF sensor regarding relative sensitivity, confinement loss, effective area, NA, birefringence and dispersion.

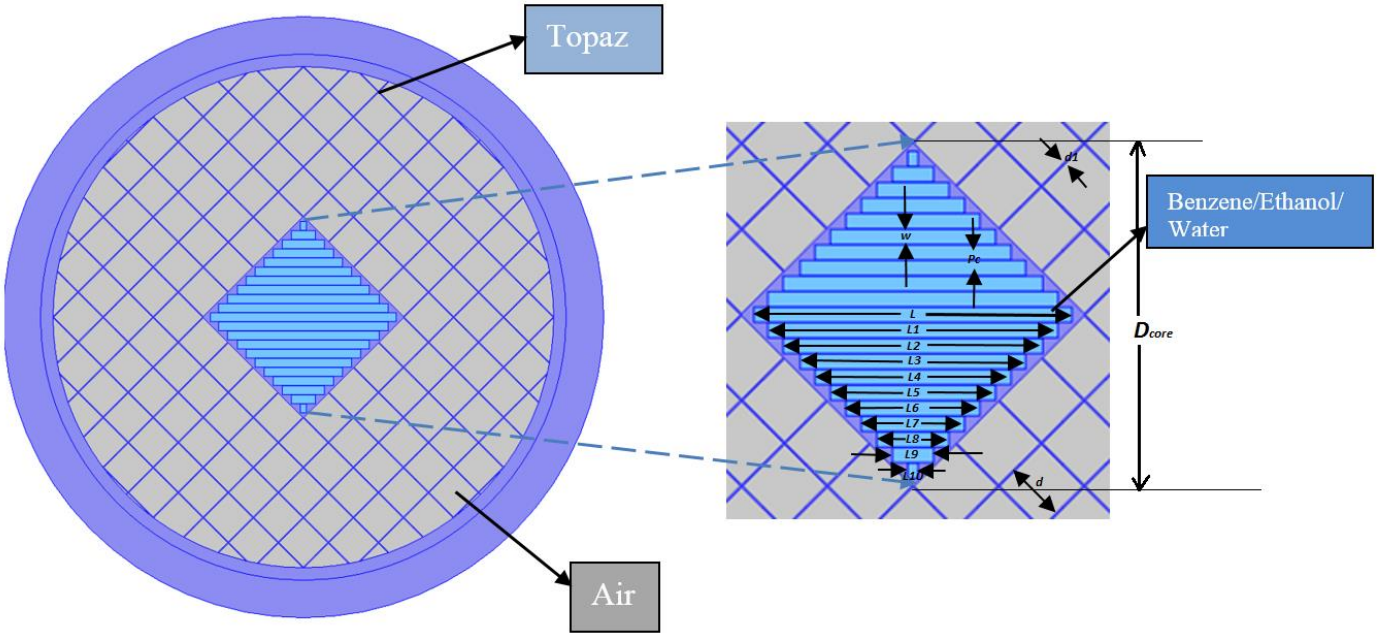

Fig. 7.2: Cross section of the proposed terahertz PC-PCF sensor with its enlarged version of the core.

In this chapter, we tried to sort out the lacking's faced by the previously proposed [65]-[72] sensors. For that, a novel PCF based chemical sensor is proposed in the terahertz frequency range. Topaz has been given as the background material of the proposed sensor. The main research goals are to achieve high relative sensitivity, negligible confinement loss, ultra-flat near zero dispersion variation, high birefringent, large effective area, as well as higher value of numerical aperture. To achieve the goal, we propose an asymmetrical rectangular structure inside the core of a square lattice PCF. We use, water, ethanol and benzene in the core air holes. The light interaction between the light and analytes are maintained using the Modified Total Internal Reflection (MTIR) technique as the refractive index of the core is greater than of cladding. The practical implementation of the fiber is feasible by means of the current fabrication technique.

7.2 Materials We Used

We have chosen materials depending on their optical properties. Topaz is the background material and three different fluids are used for filling up the core. We have used benzene, water and ethanol for core designing.

7.2.1 Background Material

Topaz was chosen as the background material of the proposed PC-PCF sensor because of its unique optical properties like constant index of refraction (n = 1.53) over a broad frequency range, low material absorption loss of 0.2 cm^{-1}, high heat resistance, high glass transition temperature, excellent water vapor barrier properties, high strength, high light transmission (91%) negligible material dispersion and humidity insensitive etc.

At TOPAS Advanced Polymers, we deliver advanced plastic materials that enable product designers and manufacturers to take a step beyond the ordinary. Our TOPAS® COC resins are a chemical relative of polyethylene and other polyolefin plastics. But they offer a lot more. TOPAS cyclic olefin copolymers are ultra-pure, crystal-clear materials with a wide range of unique properties that enable our customers to surpass the competition.

Key properties and uses of TOPAS COC resin grades include:

- **Purity**: from direct drug contact to food packaging films, TOPAS COC medical plastics have very broad global regulatory approval
- **Glass-Clear**: lightweight optics, sparkling films, glass-like healthcare containers, and high-performance diagnostics with UV transparency
- **Amorphous**: heat resistance in PCR plates, packaging, sterilizable devices and more, plus thermoformability

- **Olefin**: compatible blends with polyethylene, often with improved reclaim and recycle characteristics for sustainability
- **Barrier**: resists moisture, alcohols, acids and more for product protection in foods, medicine, and electronics

COC exhibits a unique combination of properties, which can be customized by varying the chemical structure of the copolymer. Performance benefits include:

- Low density
- High transparency
- Low birefringence
- Extremely low water absorption
- Excellent water vapor barrier properties
- Adjustable heat deflection temperature up to 170 °C
- High rigidity, strength and hardness
- Excellent biocompatibility
- Very good melt processability/flowability
- High resistance to acids and alkalis
- Very good electrical insulating properties

In the rectangular holes of the core region we inserted different chemicals like water, ethanol and benzene instead of air and observed the characteristics like relative sensitivity, confinement loss, birefringence, effective area, dispersion and numerical aperture of the fiber in terahertz frequency region.

The refractive index of water, ethanol and benzene are 1.33, 1.356 and 1.366 respectively.

7.3 Design Methodology

In Fig. 7.2 the proposed terahertz sensor is shown. In various distinctive PCF sensors, it is important as well as challenge to preserve the polarization state [68]. It is difficult to maintain the polarization states in circular shaped air holes in the core due to various factors as mentioned in [73]. So, in order to preserve the polarization state effectively it is necessary to apply asymmetric air holes in the PCF. Several PC-PCF with asymmetric structured air holes was proposed [68], [72] earlier but none of them achieved high birefringence with high relative

sensitivity. Keeping that in mind, we propose rectangular structured air holes inside the core with square cladding. The rectangular structure is responsible to increase the birefringence and compact geometry of the PC-PCF is responsible for high sensitivity as well as flat dispersion characteristics. We choose square structure in the cladding because it offers three times superior transmission bandwidth as well as very low confinement loss in a broad frequency range [76] than Bragg fibers [75]. We used COMSOL Multiphysics software to design and simulate the fiber. In Fig. 7.2, D_{core} shows the diameter of the core, the centre to centre distance between two air holes in the core region is denoted by P_c which is also known as core pitch, w indicates the core air hole width, and L, L_1, L_2, L_3, L_4, L_5, L_6, L_7, L_8. L_9 and L_{10} indicates the lengths of the core air holes which are 788 μm, 720 μm, 644 μm, 560 μm, and 486 μm 409 μm, 332 μm, 256 μm,179 μm, 102 μm and 25.6 μm respectively. The optimum values of D_{core}, P_c and w are 850 μm, 38.7 μm and 37.3 μm respectively. For the square region, the distance between parallel struts and the strut width and are defined as d and d_1. Their optimum diameters are 150 μm and 4 μm respectively. Topaz was chosen as the background material of the proposed PC-PCF sensor because of its unique optical properties like constant index of refraction (n = 1.53) over a broad frequency range, low material absorption loss of 0.2 cm^{-1}, high heat resistance, high glass transition temperature, excellent water vapour barrier properties, high strength, high light transmission (91%) negligible material dispersion and humidity insensitive [77] etc.

In the rectangular holes of the core region we inserted different chemicals like water, ethanol and benzene instead of air and observed the characteristics like relative sensitivity, confinement loss, birefringence, effective area, dispersion and numerical aperture of the fiber in terahertz frequency region. The refractive index of water, ethanol and benzene are 1.33, 1.356 and 1.366 respectively [69].

7.4 Synopsis of The Numerical Method

The most powerful widely used full vector Finite Element Method (FEM) available to the engineers and other research community to analyze the characteristics of photonic devices is used to characterize our proposed PC-PCF sensor [77]-[80].

To understand the performance of the proposed PC-PCF into sensing applications, it is important to calculate the relative sensitivity. Sensitivity is a measure of the amount of

interaction of light with the material need to be sensed. It can be expressed by using the modified Beer Lambert Law that can be expressed as [60],

$$R = \frac{n_r}{n_{eff}} \times e \quad \text{..... (7.1)}$$

where, R is defined as the relative sensitivity, n_r is refractive index of the chemical need to be detected, n_{eff} represents the effective refractive index, and e can be defined as the amount of energy presents in the core holes.

According to Poyntings theorem the equation of calculating the fraction of power presents in the core holes can be defined as [60],

$$e = \frac{\int_{sample} R_e(E_x H_y - E_y H_x) dxdy}{\int_{total} R_e(E_x H_y - E_y H_x) dxdy} \times 100 \quad \text{..... (7.2)}$$

here, e represents the percentage of interaction of light with the chemicals in the core holes to be sensed, E_x, E_y and H_x, H_y are the transverse electric and magnetic fields of the guided mode respectively. The integration of numerator of Eqn. 2 is done over the chemicals to be sensed in the core region and the integration of the denominator is done over the whole fiber region.

Preserving the polarization state of a PC-PCF is also important in consideration to sensing applications; eliminating the polarization mode dispersion (PMD), as well as stabilizing the operation of optical devices. Birefringence is a measure of the polarization states of a fiber that is defined as the refractive index difference between the polarization modes. It can be calculated by the following equation,

$$B = |n_x - n_y| \quad \text{..... (7.3)}$$

here, B indicates the birefringence, n_x represents the mode index in the x-polarization mode and n_y represents the mode index in the y-polarization mode.

Confinement loss of an optical link is also an important parameter that specifies the length of signal transmission. It depends upon the core porosity as well as the number of rings used in the cladding [55]. It can be mentioned that, during the simulation leakage of useful light happens from the core to the cladding. This amount of light leakage determines the confinement

loss that can be calculated using the imaginary part of the complex refractive index using the equation [55],

$$L_c = \left(\frac{4\pi f}{c}\right) Im\left(n_{eff}\right), cm^{-1} \quad \text{..... (7.4)}$$

Here, L_c indicates the confinement loss, f specifies the operating frequency, and $Im(n_{eff})$ represents the imaginary part of the effective refractive index.

In order to use the PC-PCF in a multichannel communication link the dispersion characteristics should be as flat as possible. If the fiber gets a flattened dispersion property, several signal from the source arrives at the destination nearly at the same rate. As discussed earlier, Topaz has been selected as the base material of our proposed PC-PCF sensor and according to the characteristics of Topaz we only calculated the waveguide dispersion because the material dispersion is negligible in Topaz [55]. The dispersion parameter of a fiber can be calculated using the equation [52],

$$\beta_2 = \frac{2}{c}\frac{dn_{eff}}{d\omega} + \frac{\omega}{c}\frac{d^2 n_{eff}}{d\omega^2}, \text{ ps/THz/cm} \quad \text{.....(7.5)}$$

Here, β_2 indicates the dispersion, c indicates the speed of light, ω indicates the radian frequency. The area covered by the mode fields inside the core region can quantitively be measured by the term effective area. The effective area of a fiber can be calculated by [54],

$$A_{eff} = \frac{[\int I(r) r dr]^2}{[\int I^2(r) r dr]^2} \quad \text{..... (7.6)}$$

here, $I(r) = |E_t|^2$ represents the amount of electric field spreading in the transverse of the PC-PCF.

Numerical Aperture (NA) of an optical fiber sensor is a very important parameter that is required for optical coherence tomography (OCT) in medical imaging applications [82]. OCT is a non-invasive medical imaging test that uses light wave to capture micrometer resolution three-dimensional image from optical scattering media of human body. This is basically done

by the reflection of light from the biological tissue [81]. Large value of NA is suitable for medical imaging that can be achieved when the refractive index difference between the core and cladding of a PCF can be made larger. It can be mentioned that, it is uncommon to find a silica fiber having a NA above 0.40 [83]. In our proposed PC-PCF, we tried to increase the NA using our novel geometrical structure in sensing application and having Topaz as the background material. NA can be quantified by the following equation [82],

$$NA = \frac{1}{\sqrt{1+\frac{\pi A_{eff} f^2}{c^2}}} \quad \text{..... (7.7)}$$

Here, A_{eff} represents the effective area of the proposed PCPCF sensor.

7.5 Simulation Results and Discussion

The intensity of light interaction with the chemicals (water, ethanol & benzene) is shown in Fig. 2. It can be seen that light is strongly interact with the chemicals used inside the core holes. To characterizes the modal characteristics, we can observe the light propagation for both *x* and *y* polarization mode.

It can be seen that only the fundamental modes are transferring through the core area. However, as the wave-guide structure is asymmetry so there may have some birefringence and some different modes can be present but for those modes the light will be propagated outside the core area [84]. So, when a light pulse emerged at the center of the waveguide only the fundamental modes will be excited and PC-PCF sensor will operate into the single mode condition.

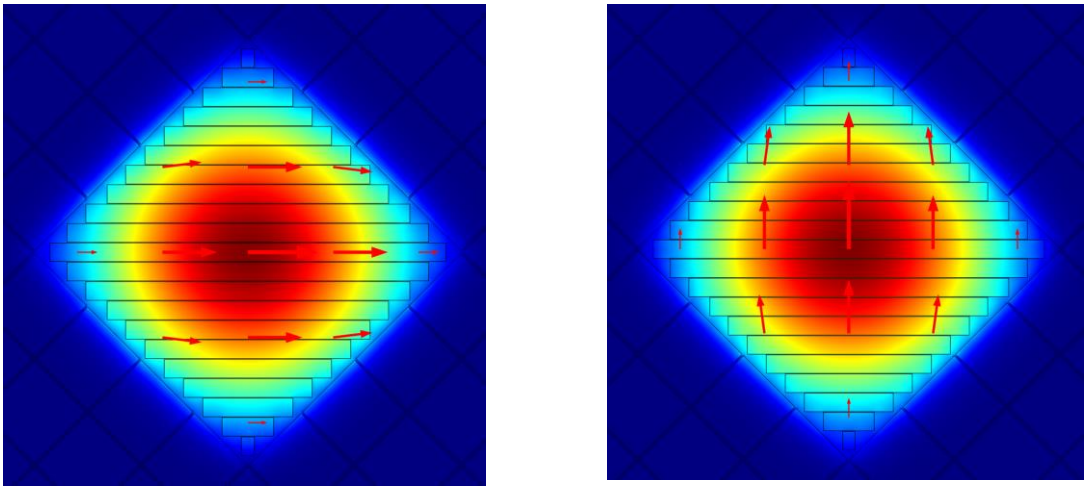

(a) (b)

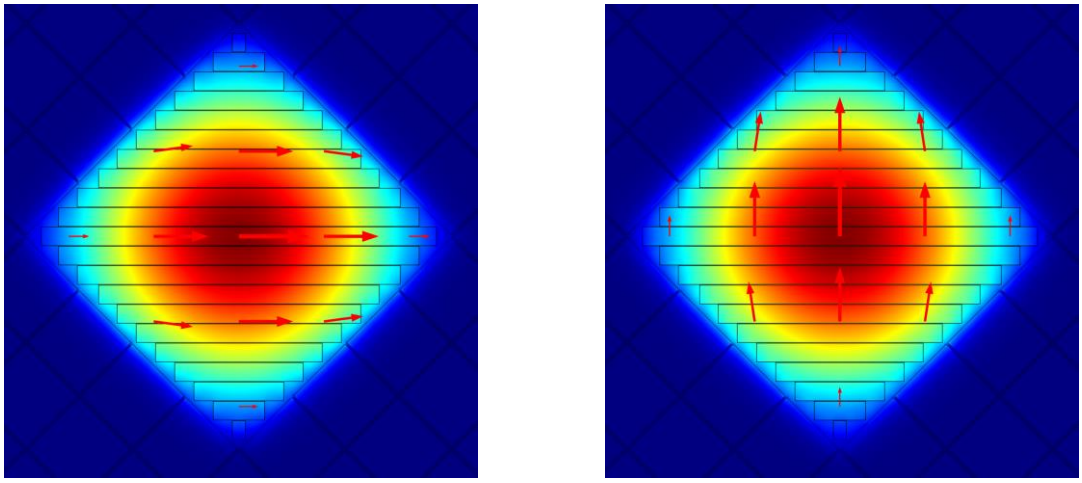

(c) (d)

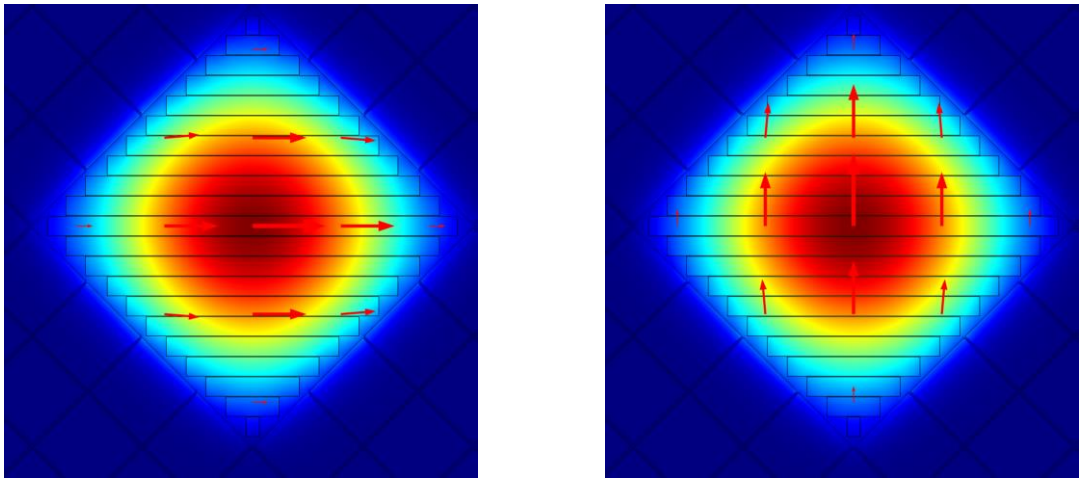

(e) (f)

Fig.7.3: Mode power distribution of the proposed PC-PCF for (a) water, *x*-pol (b) water, *y*-pol (c) ethanol, *x*-pol (d) ethanol, *y*-pol (e) benzene, *x*-pol (f) benzene, *y*-pol

The relative sensitivity of the proposed PC-PCF as a function of frequency and in the *x*-polarization mode is shown in Fig. 8.4. The length and height of the slotted holes in the core region were kept fixed for all numerical simulations.

Three different analytes were used to test the sensitivity of the proposed chemical sensor. The analytes are water (n = 1.33), ethanol (n = 1.356), and benzene (n = 1.36). It can be seen from Fig. 8.4 that the chemical benzene got a highest relative sensitivity because of its high refractive index than water and ethanol.

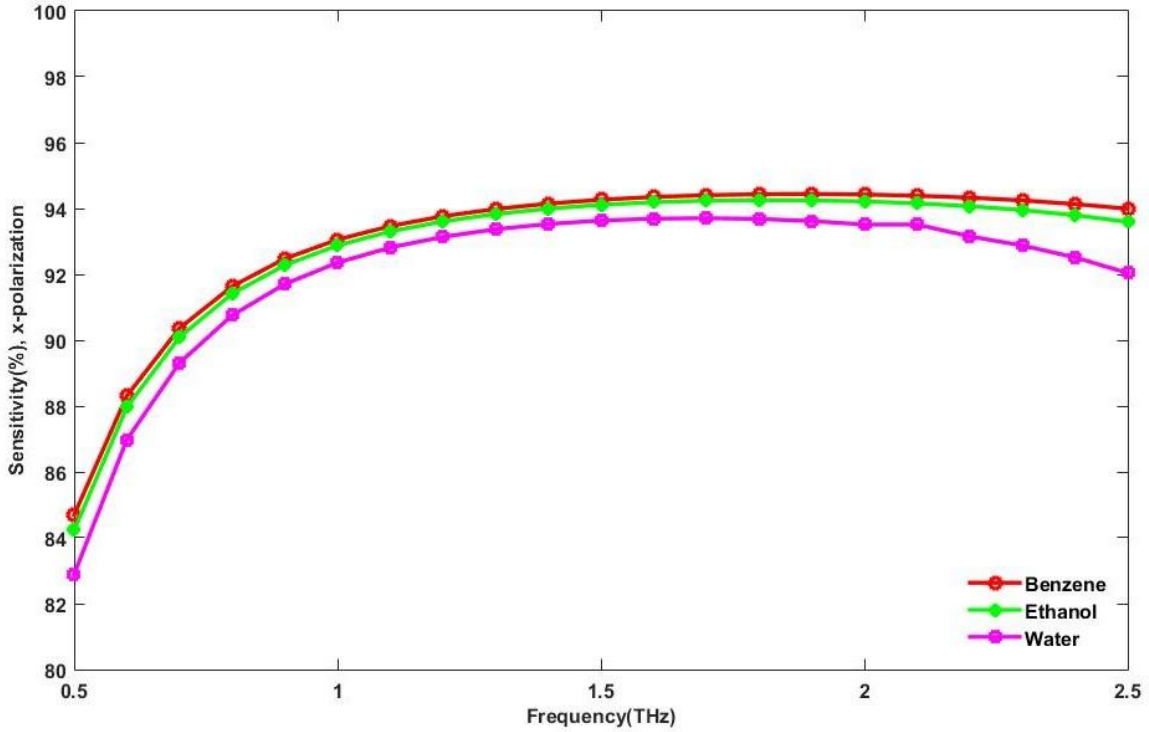

Fig. 7.4: Relative Sensitivity of water, ethanol & benzene as a function of frequency at *x*-polarization mode.

It can also be observed that, relative sensitivity increases with frequency up to 1.8 THz and then starts to decrease. This is true, as the frequency increases from 0.5 THz the interaction of light with the chemicals also increases and light interaction reaches its maximum position at 1.8 THz.

Further increment in frequency causes some of the useful power penetrates towards the cladding and background material and thus light interaction with the chemicals decreases that in turn reduces the relative sensitivity. So, at 1.8 THz, 37.3 μm slotted hole width and *x*-polarization mode the relative sensitivity for water, ethanol and benzene are 93.68%, 94.25%, and 94.43% respectively.

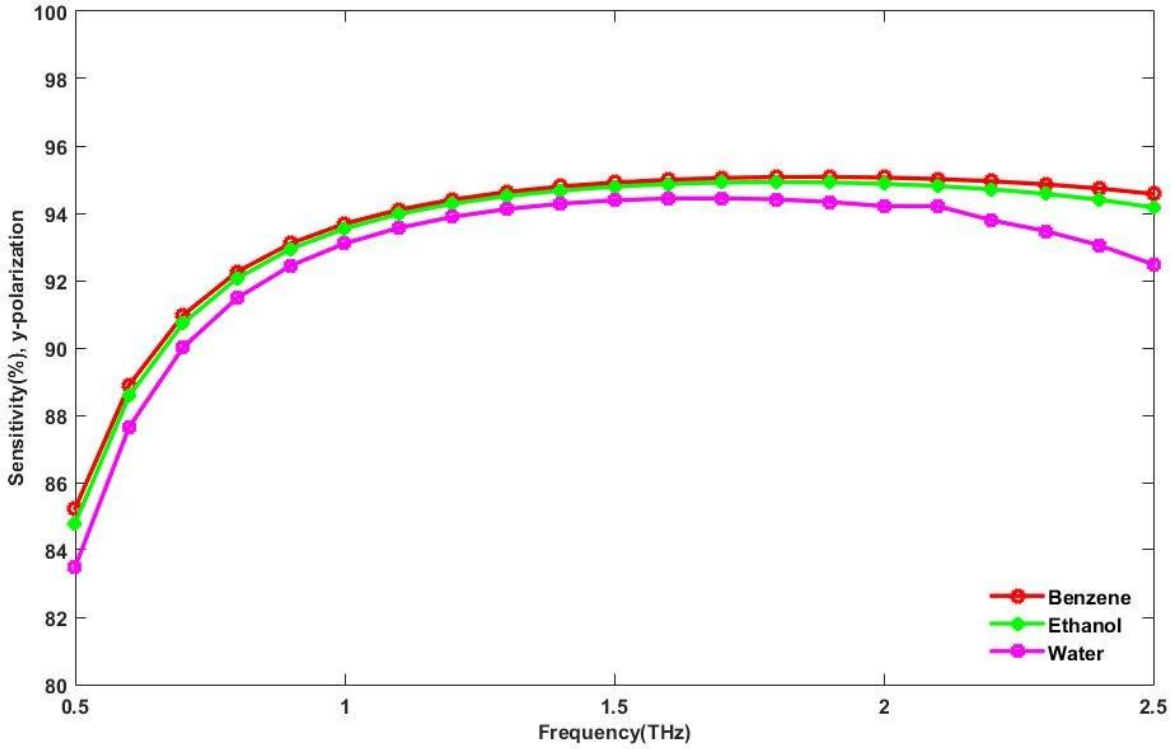

Fig. 7.5: Relative Sensitivity of water, ethanol benzene as a function of frequency at *y*-polarization mode.

Keeping all the parameters same next we calculated the relative sensitivity of the proposed sensor for the *y*-polarization mode. From Fig. 8.5 it can be seen that, sensitivity in the *y* polarization mode increases than the *x*-polarization because light is well interact in the *y*-polarized mode than the *x* polarization. We can get the proof of it from Fig. 8.2 where it is clearly observed that the interaction of light and analytes is better in *y*-polarization mode than the *x*-polarization mode. For this reason, we choose *y*-pol as optimum for our proposed PC-PCF sensor.

The relative sensitivity obtained for the *y* polarization for water, ethanol and benzene are 94.4%, 94.92%, and 95.09% respectively. To the best of our knowledge, this is the highest relative sensitivity obtained for any kind of sensor proposed for chemical sensing application in terahertz frequency range.

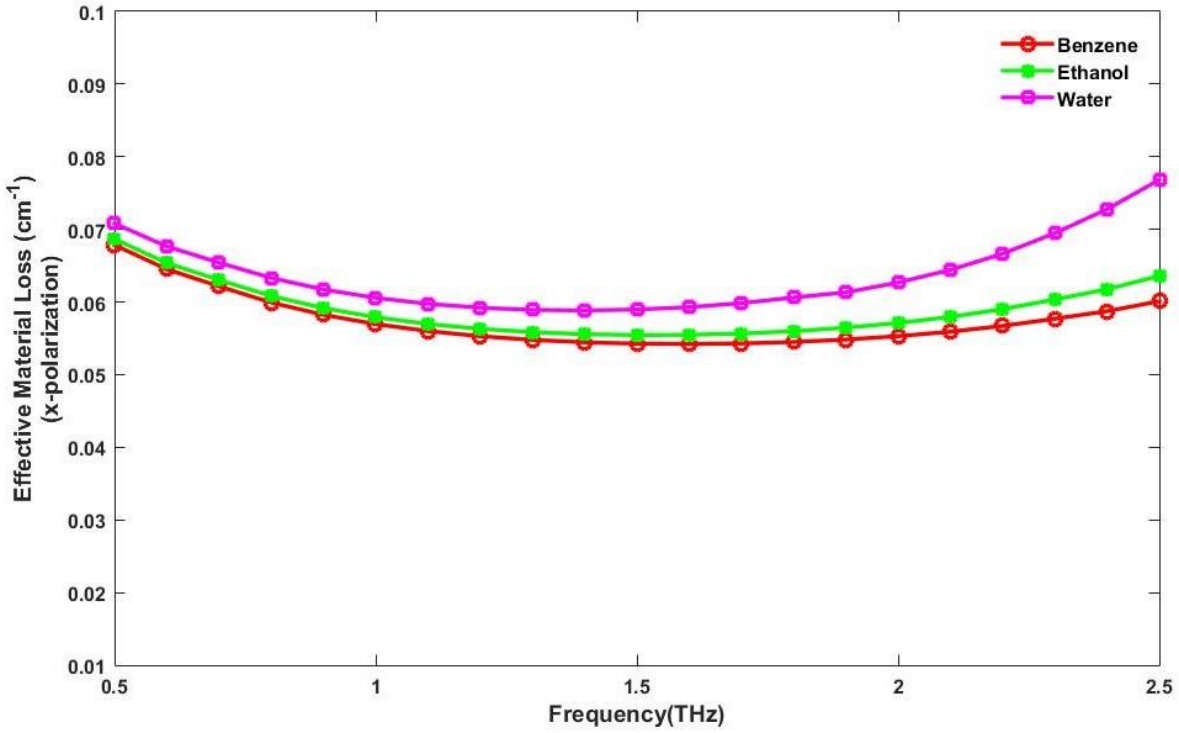

Fig. 7.6: Effective Material Loss (EML) of water, ethanol benzene as a function of frequency at x-polarization

The graph is showing that when increasing frequency from 0.5THz to higher value EML is reducing for all the materials up to 1.6 to 1.8THz frequency at x-polarization.

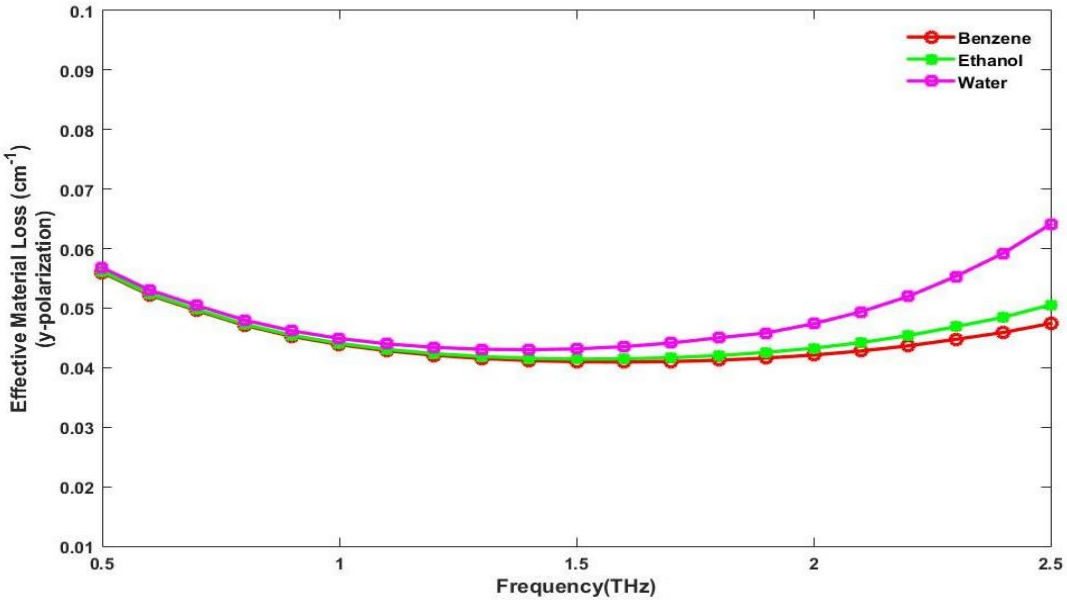

Fig. 7.7: Effective Material Loss (EML) of water, ethanol benzene as a function of frequency at y-polarization

The characteristics of birefringence with respect to frequency is shown in Fig. 8.8. It is observed that, a linear birefringence value is obtained all over the frequency region.

The interaction of the evanescent field with the sensing chemicals increases with frequency and thus the confinement loss decrease. The obtained confinement loss for water, ethanol and benzene are $4.5649 \times 10^{-9}\,\mathrm{cm}^{-1}$.

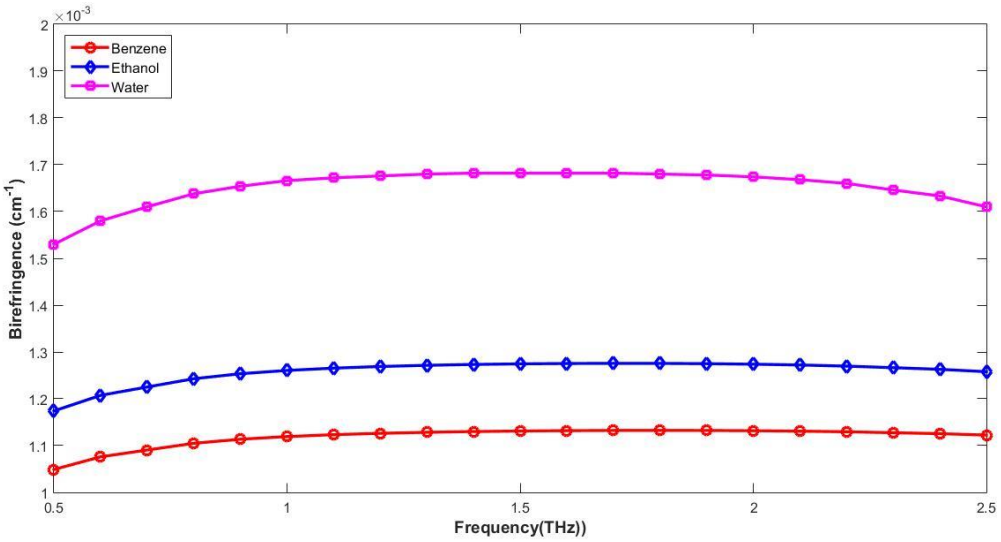

Fig. 7.8: Birefringence of water, ethanol benzene as a function of frequency optimum design parameters

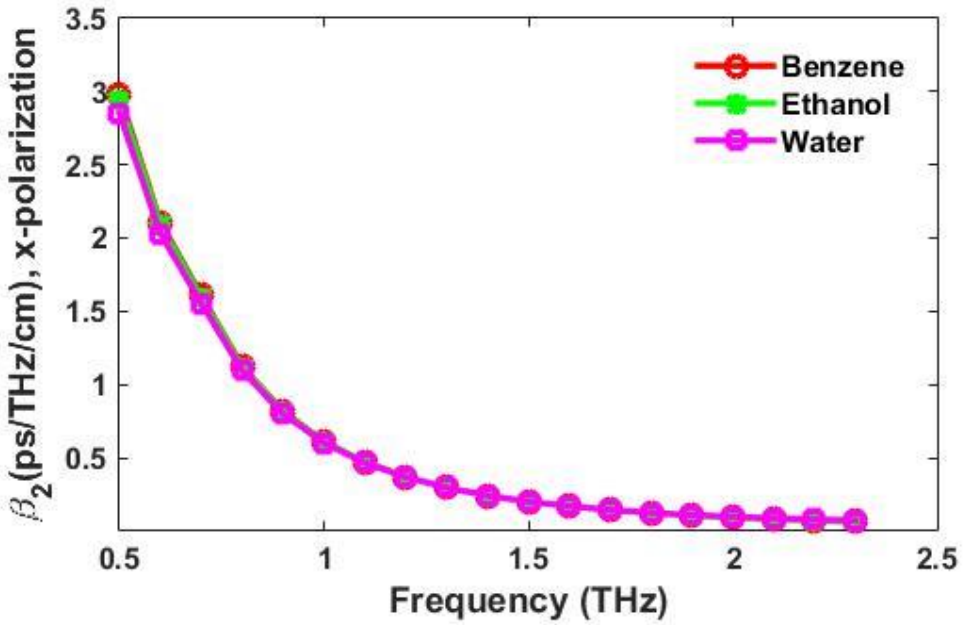

Fig.7.9: Dispersion as a function of frequency at optimum design parameters at x-polarization mode.

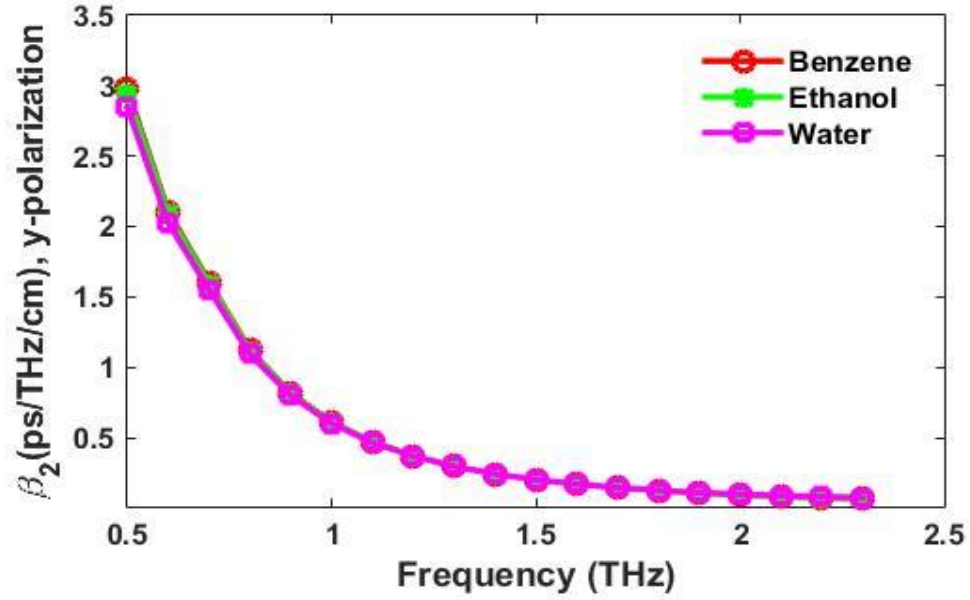

Fig.7.10: Dispersion as a function of frequency at optimum design parameters at y-polarization mode.

The feature of dispersion of the proposed sensor for different chemicals is shown in Fig. 7.9 and Fig. 7.10. Dispersion is an important optical property that were ignored to discuss in the previously proposed fibers [65]-[72] for sensing application.

The behavior of effective area as a function of frequency is shown in Fig. 8.11 and Fig. 8.12. It can be observed that, effective area decreases with frequency as light pulses are narrowly remarked in the porous core region with frequency increase.

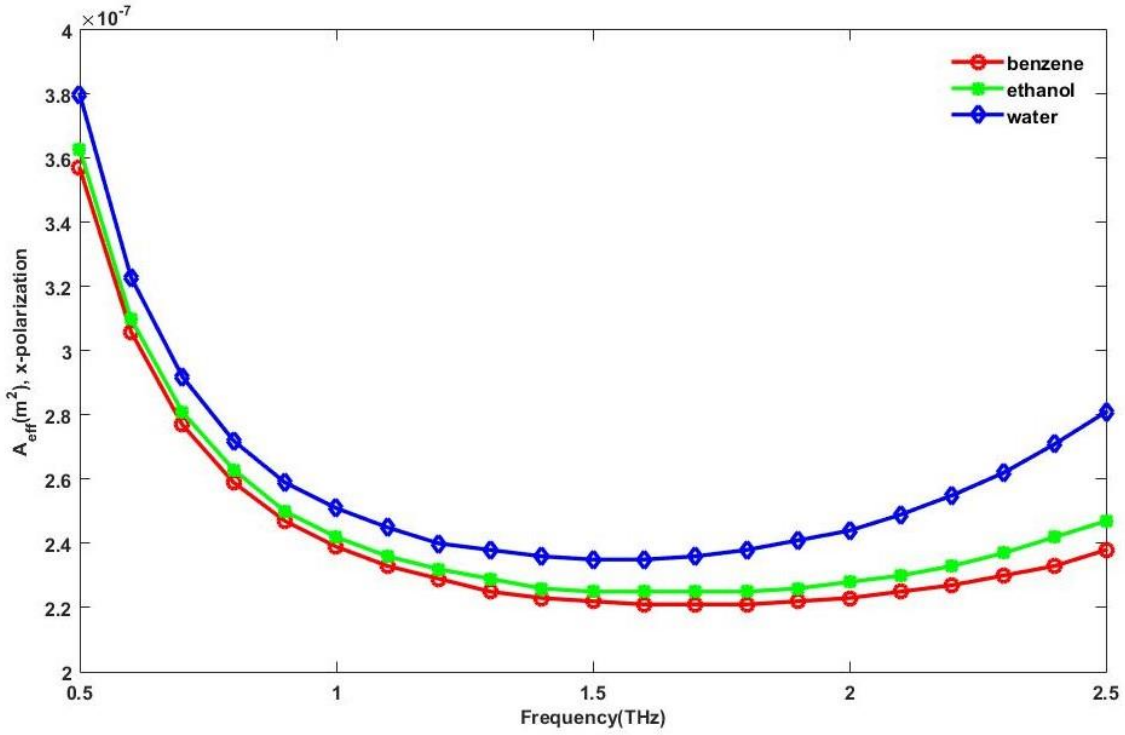

Fig. 7.11: Effective area as a function of frequency at optimum design parameters at x-polarization mode.

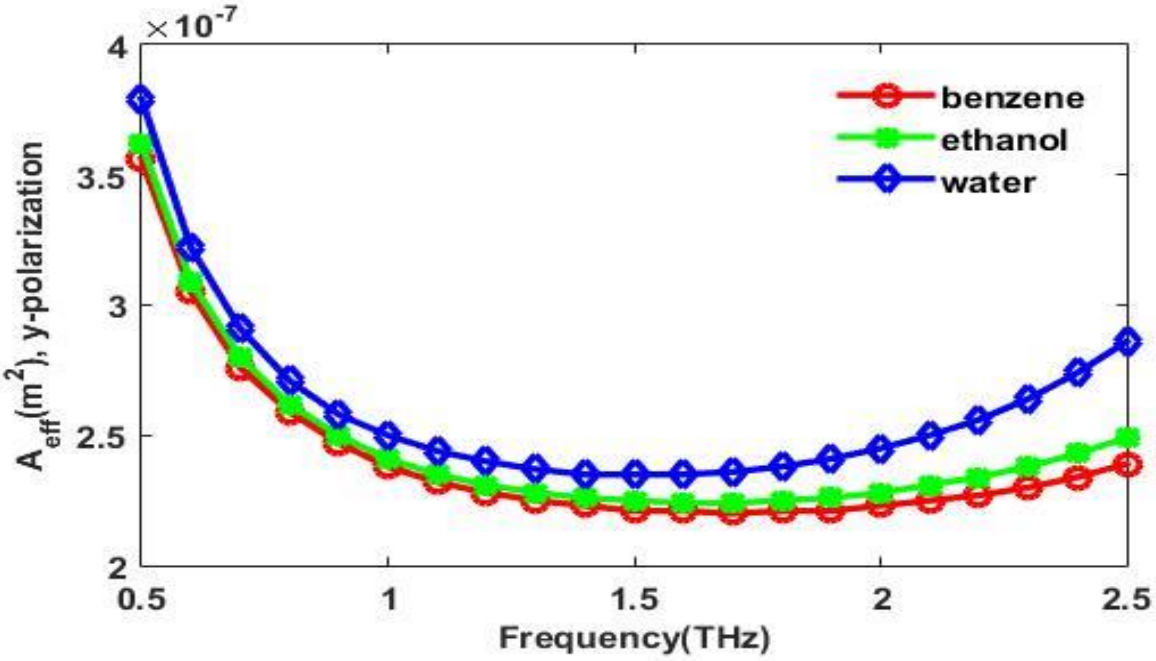

Fig.7.12: Effective area as a function of frequency at optimum design parameters at y-polarization mode.

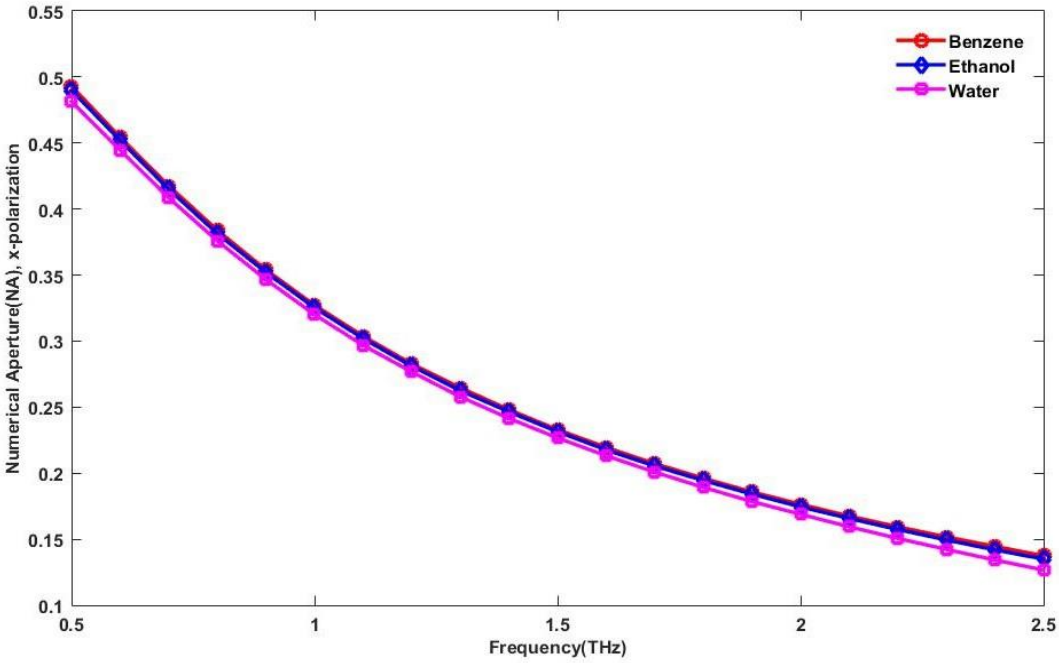

Fig. 7.13: Numerical Aperture as a function of frequency at optimum design parameters at x-polarization mode.

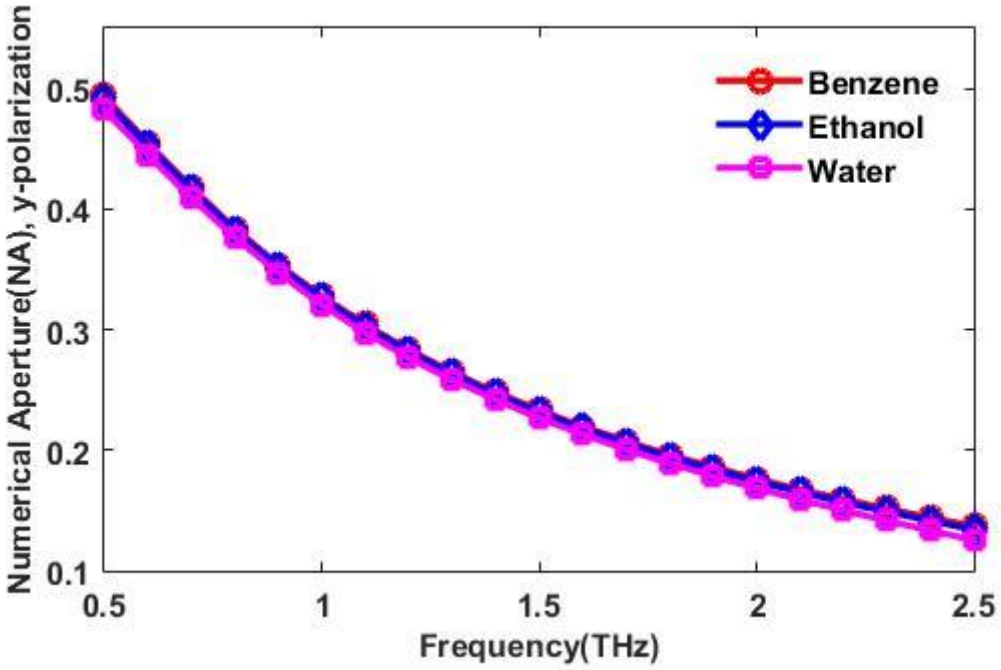

Fig. 7.14: Numerical Aperture as a function of frequency at optimum design parameters at y-polarization mode.

The characteristics of Numerical Aperture with frequency variation and other optimal design parameters are shown in Fig. 8.13 and Fig. 8.14. It can be seen that numerical aperture decreases with frequency. A high value of NA is obtained at 1 THz frequency however as the main concern of the proposed PC-PCF is to increase the sensitivity so we choose 1.8 THz as optimum.

7.6 Fabrication

Fabrication is the most important part of a fiber design in which the practical application of a PCF is totally dependent. There are a number of well-developed fabrication technologies available now a days to fabricate any types of fiber structure. 3D-printing, extrusion, capillary stacking, stack and drilling and sol-gel are the most common. As our proposed PCPCF consists of asymmetrical structure so capillary stacking and sol-gel are not suitable to fabricate the proposed fiber as they can only fabricate circular shaped micro structured air holes. However,

it is worthwhile to note that, square lattice PC-PCF with asymmetrical rectangular structured hole based core has already been fabricated by Atakaramians *et. al.* [85]. Moreover, kagome lattice PCF with different complex structur have also been fabricated by the Max Plank Institute [86]. Moreover, for sensing and photochemistry applications a kagome lattice PCF including some other complex PCF structures had been fabricated by Cubillas *et. al.* [87]. So, using the existing PCF fabrication technologies the proposed PCF is feasible to fabricate.

CHAPTER 8
CONCLUSIONS

8.1 Conclusion

A square lattice slotted core micro-structured PC-PCF based chemical sensor is proposed for terahertz sensing applications. Using Topaz as the base material the simulation result shows an ultra-high relative sensitivity of 94.4%, 94.9%, and 95% for water, ethanol and benzene respectively in the terahertz frequency range.

Terahertz radiation occupies a middle ground between microwaves and infrared light waves known as the terahertz gap**,** where technology for its generation and manipulation is in its infancy. The frequency band of 0.1-10 THz, known as THz band has brought potential applications in many important fields.

For wave propagation THz systems use free space as medium. But in free space waves face many difficulties which is very big issue for wave propagation. So, we have to use guided transmission instead of unguided transmission.

In the meantime, many guided transmission lines have many kinds of deprivation such as effective material loss (EML), confinement loss, bending loss, dispersion loss, power fraction issue etc.

A highly sensitive porous core – photonic crystal fiber (PC-PCF) has been designed and analyzed for remote detection of chemical analytes in terahertz frequency range. The PC-PCF has been modelled using rectangular structured air holes in the core with square structured cladding. The full vectorial finite element method (FEM) has been used to tune the geometrical parameters also to characterize the fiber.

At 1.8 THz, 37.3 μm slotted hole width and *x*-polarization mode the relative sensitivity for water, ethanol and benzene are 93.68%, 94.25%, and 94.43% respectively. The relative sensitivity obtained for the *y* polarization for water, ethanol and benzene are 94.4%, 94.92%, and 95.*0*9% respectively. Effective Material Loss (EML) of water, ethanol benzene at frequency 1.8THz at x-polarization 0.06 cm^{-1}, 0.055 cm^{-1}, 0.054 cm^{-1} respectively. Effective Material Loss (EML) of water, ethanol benzene at frequency 1.8THz at y-polarization 0.044 cm^{-1}, 0.0411 cm^{-1}, 0.054 cm^{-1} respectively. Effective area at optimum design parameters at x-polarization mode are 2.38E-07m^2, 2.25E-07m^2 and 2.21E-07m^2 at y-polarization mode are 2.38E-07m^2, 2.25E-07m^2 and 2.21E-07m^2 for water, ethanol and benzene respectively.

Simulation results demonstrate a high relative chemical sensitivity for different analytes. Moreover, the PCF shows very low near zero dispersion variation, high modal effective area, high birefringence and high numerical aperture (NA). The practical implementation of the fiber is feasible with the present fabrication techniques. The optimized PCF with such attractive characteristic has commercial applications in remote chemical sensing as well as polarization preserving applications of terahertz waves.

Moreover, near zero flat dispersion, high birefringence, high effective area and high numerical aperture has also been obtained at optimal design parameters. The proposed PC-PCF sensor is realizable using the existing fabrication technology. Thus, it is expected that, with such remarkable sensing properties the proposed PC-PCF based sensor opens a new window for further terahertz sensor research and paves the way to mitigate the necessities of a chemical sensor for chemical sensing and other biological applications.

8.2 Drawback and Future Proposal

An immensely lower effective material loss, notably marginal core power fraction, less confinement loss and near zero ultra-flat dispersion has been introduced in our proposed design. In our proposed design, single mode properties have also been satisfied and designed for THz wave guidance. For the first time square cladding and slotted square core has been introduced which helps us to reduce the effective material loss and preferably for a margin of core power fraction.

The primary implication of our proposed structure is its simplicity and loss reduction. Our proposed design contains attractive guiding properties which will be significant for THz wave application. For long distance communication of THz signal, our proposed design can be used relevantly.

The main drawback of our proposed design is power fraction can further be increased & EML can further be decreased. Still the accumulated result is satisfactory & can be developed in future for practical purpose.

So, the future goal should be developing a fabrication process for this accumulated design which is efficient & easy so that worldwide it can be adopted. Furthermore, simulations should be continued for new designs so that low EML & high-power fraction design can be adopted & fabricated practically.

REFERENCES

[1] K. Wang and D. M. Mittleman, ‘‘Metal wires for terahertz wave guiding,’’ nature 432, 376–379 (2004).

[2] B. Bowden, J. A. Harrington, and O. Mitrofanov, ‘‘Silver/polystyrene-coated hollow glass waveguides for the transmission of terahertzradiation,’’opt. lett. 32(20), 2945–2947 (2007).

[3] C. Themistos et al., “Characterization of silver/polystyrene (PS) coated hollow glass waveguides at THz frequency,”J. Lightwave Technol.25(9), 2456–2462 (2007).

[4] M. Skorobogatiy and A. Dupuis, “Ferroelectric all-polymer hollow Bragg fibers for terahertz guidance,” Appl. Phys. Lett., vol. 90, no. 11,pp. 113514-1–113514-3, Mar. 2007.

[5] M. Skorobogatiy and A. Dupuis, “Ferroelectric all-polymer hollow Bragg fibers for terahertz guidance,” Appl. Phys. Lett., vol. 90, no. 11,pp. 113514-1–113514-3, Mar. 2007.

[6] L. J. Chen et al., “Low-loss subwavelength plastic fiber for terahertz waveguiding,” opt. Lett. 31(3), 308–310 (2006).

[7] L.J.Chen, H.W. Chen, T.F.Kao, J.Y. Lu,and C.K. Sun,“Low-loss subwavelength plastic fiber for terahertz waveguiding,” Opt. Lett., vol. 31, no. 3, pp. 308–310, Feb. 2006.

[8] M. Nagel, A. Marchewka, and H. Kurz, “Low-index discontinuity terahertz waveguides,” Opt. Express, vol. 14, no. 21, pp. 9944–9954, 2006

[9] L.J. Chen, H.W. Chen, T.F. Kao, J.Y. Lu, C.K. Sun, “Low-loss subwavelength plasticfiber for terahertz waveguiding”, Opt. Lett. 31 (3) (2006) 308–310.

[10] C.S. Ponseca Jr., R. Pobre, E. Estacio, N. Sarukura, A. Argyros, M.C. Large, M.A. van Eijkelenborg, “Transmission of terahertz radiation using a microstructuredpolymer optical fiber”, Opt. Lett. 33 (9) (2008) 902–904.

[11] K. Nielsen, H.K. Rasmussen, A.J. Adam, P.C. Planken, O. Bang, P.U. Jepsen,

[12] Bendable, “low-loss Topas fibers for the terahertz frequency range”, Opt. Exp. 17(10) (2009) 8592–8601.

[13] M. Goto, A. Quema, H. Takahashi, S. Ono, N. Sarukura, “Teflon photonic crystal fiber as terahertz waveguide”, Jpn. J. Appl. Phys. 43 (2B) (2004) L317–L319. pt.2.

[14] G. Zhao, M.T. Mors, T. Wenckebach, P.C.M. Planken, “Terahertz dielectricproperties of polystyrene foam”, J. Opt. Soc. Amer. B 19 (6) (2002) 1476–1479.

[15] J.Y. Lu, C.P. Yu, H.C. Chang, H.W. Chen, Y.T. Li, C.L. Pan, C.K. Sun, “Terahertz air-core microstructure fiber”, Appl. Phys. Lett. 92 (6) (2008) 064105-1–064105-3

[16] M. Skorobogatiy, A. Dupuis, “Ferroelectric all polymer hollow Bragg fibers for terahertz guidance”, Appl. Phys. Lett. 90 (11) (2007) 113514-1–113514-3.

[17] H. Han, H. Park, M. Cho, and J. Kim, “Terahertz pulse propagation in a plastic photonic crystal fiber,” Appl. Phys. Lett., vol. 80, no. 15, pp. 2634–2636, 2002.

[18] P.J.St. Russell, “Photonic crystal fibers”, Science 299 (5605) (2003) 358–362.

[19] H. Han, H. Park, M. Cho, J. Kim, “Terahertz pulse propagation in a plastic photonic crystal fiber”, Appl. Phys. Lett. 80 (15) (2002) 2634–2636.

A. Hassani, A. Dupuis, M. Skorobogatiy, “Porous polymer fibers for low-loss terahertz guiding”, Opt. Express 16 (9) (2008) 6340–6351.

B. Ung, A. Mazhorova, A. Dupuis, M. Roze, M. Skorobogatiy, “Polymer microstructured optical fibers for terahertz wave guiding”, Opt. Express 19(26) (2011) B848–B861.

[20] K. Nielsen, H.K. Rasmussen, P.U. Jepsen, O. Bang, “Porous-core honeycomb bandgap THz fiber”, Opt. Lett. 36 (5) (2011) 666–668.

[21] H. Bao, K. Nielsen, H.K. Rasmussen, P.U. Jepsen, “Fabrication and characterization of porous-core honeycomb bandgap THz fibers”, Opt. Express20 (28) (2012) 29507–29517.

[22] M. Uthman, B.M.A. Rahman, N. Kejalakshmy, A. Agarwal, K.T.V. Grattan, “Design and characterization of low-loss photonic crystal fiber”, IEEE photonics J. (6)(2012).

[23] S. Atakaramians, S. A. Vahid, B. M. Fischer, D. Abbott, and T. M. Monro, “Porous fibers: A novel approach to low loss THz waveguides,” Opt. Exp., vol. 16, no. 12, pp. 8845–8854, Jun. 2008.

[24] S. F. Kaijage, Z. Ouyang, and X. Jim, “Porous-core photonic crystal fiber for low loss terahertz wave guiding”,IEEE Photon. Technol. Lett.,vol. 25, no. 15, pp.1454–1457, Aug. 1, 2013.

[25] M. Uthman, B.M.A. Rahman, N. Kejalakshmy, A. Agarwal, K.T.V. Grattan, "Design and characterization of low-loss photonic crystal fiber", IEEE photonics J 4(6)(2012).

[26] K. Nielsen, H. K. Rasmussen, P. U. Jepsen, and O. Bang, "Porous-core honeycomb

[27] bandgap THz fiber," Opt. Lett., vol. 36, no. 5, pp. 666–668, Mar. 2011.

[28] M. Uthman, B.M.A. Rahman, N. Kejalakshmy, A. Agarwal, K.T.V. Grattan, Design and characterization of low-loss photonic crystal fiber, IEEE photonics J. 4 (6) (2012).

[29] J. Liang, L. Ren, N. Chen, and C. Zhou, "Broadband, low-loss, dispersion flattened porous-core photonic bandgap fiber for terahertz (THz)- wave propagation," Opt. Commun., vol. 295, pp. 257 261, May 2013.

[30] S. F. Kaijage, Z. Ouyang, and X. Jim, "Porous-core photonic crystal fiber for low loss terahertz wave guiding,"IEEE Photon. Technol. Lett., vol. 25, no. 15, pp. 1454–1457, Aug. 1, 2013.

[31] RaonaqulIslam,G. K. M. Hasanuzzaman, Md. Selim Habib, SohelRana, M. A. G. Khan "Low-loss rotated porous core hexagonal single-mode fiber in THz regime"Elsevier Optical Fiber Technology 24 (2015) 38–43.

[32] SohelRana, GolamKibria, Md. Hasanuzzaman, Samiul Habib, Shubi F. Kaijage, Raonaqul Islam "Proposal for a low loss porous core octagonal photonic crystal fiber for T-ray wave guiding" Optical Engineering 53(11), 115107 (November 2014).

[33] Md. Imran Hasan, S. M. AbdurRazzak, G. K. M. Hasanuzzaman, Md. Samiul Habib "Ultra-Low Material Loss and Dispersion Flattened Fiber for THz Transmission" IEEE PHOTONICS TECHNOLOGY LETTERS, VOL. 26, NO. 23, DECEMBER 1, 2014

[34] Md.Saiful Islam , SohelRana, Mohammad Rakibul Islam, Mohammad Faisal, Hasan Rahman, Jakeya Sultana "Porous core photonic crystal fiber for ultra-low material loss in THz regime" IET Journals (July,2016)

[35] . Nielsen, H. K. Rasmussen, A. J. L. Adam, P. C. M. Planken, O. Bang, and P. U. Jepsen, "Bendable, low-loss Topas fibers for the terahertz frequency range," Opt. Exp., vol. 17, no. 10, pp. 8592–8601, May 2009.

[36] R. T. Bisen and D. J. Trevor, "Solgel-derived microstructured fibers: Fabrication and characterization," in Proc. Opt. Fiber Commun.Conf. (OFC), Mar. 2005, p. OWL6.

[37] Raonaqul Islam, G.K.M. Hasanuzzaman, Md. Selim Habib, Sohel Rana, "Low-loss rotated porous core hexagonal single-mode fiber in THz regime,"Optical Fiber Technology , 38-43, May 2015.

[38] M. Walther, B. M. Fischer, A. Ortner, A. Bitzer, A. Thoman, and H. Helm, "Chemical sensing and imaging with pulsed terahertz radiation," Analytical and Bioanalytical Chemistry, vol. 397, no. 3, pp. 1009– 1017, (2010).

[39] B. M. Fischer, H. Helm and P. U. Jepsen,"Chemical recognition with broadband THz spectroscopy," Proceedings of the IEEE, vol. 95, no. 8, pp. 1592–1604 (2007).

[40] B. M. Fischer, M Hoffmann, H. Helm, G. Modjesch and P. Uhd Jepsen, "Chemical recognition in terahertz time-domain spectroscopy and imaging," Semiconductor Science and Technology, vol. 20, no. 7, S246, (2005).

[41] W. Withayachumnankul, G. M. Png, X. Yin, S. Atakaramians, I. Jones, H. Lin, B. S. Y. Ung, J. Balakrishnan, B. W.-H. Ng, B. Ferguson, S. P. Mickan, B. M. Fischer, and D. Abbott, "T-ray sensing and imaging," Proceedings of the IEEE., vol. 95, no. 8, pp. 1528–1558, 2007.

[42] J. Q. Zhang and D. Grischkowsky, "Waveguide terahertz time-domain spectroscopy of manometer water layers," Opt. Lett., vol. 29, no. 14, pp. 1617-1619 (2004).

[43] M. Nagel, P. H. Bolivar, M. Brucherseifer, H. Kurz, A. Bosserhoff and R. Bttner, "Integrated THz technology for label-free genetic diagnostics," Appl. Phy. Lett., vol. 80, no. 154, pp. 154–156 (2002).

[44] B. M. Fischer, M. Hoffmann, H. Helm, R. Wilk, F. Rutz, T. KleineOstmann, M. Koch, and P. Uhd Jepsen, "Terahertz time-domain spectroscopy and imaging of artificial RNA," Opt. Express., vol. 13, no. 14, pp. 5205–5215 (2005).

A. G. Markelz, A. Roitberg, E. J. Heilweil, "Pulsed terahertz spectroscopy of DNA, bovine serum albumin and collagen between 0.1 and 2.0 THz," Chemical Physics Letters,, vol. 320, no. 1, pp. 42–48 (2000).

A. G. Markelz, J. R. Knab, J. Y. Chen, and Y. He, "Protein dynamical transition in terahertz dielectric response," Chemical Physics Letters,, vol. 442, no. 4, pp. 413–417 (2007).

B. M. Fischer, M. Walther and P. Uhd Jepsen, "Far-infrared vibrational modes of DNA components studied by terahertz time-domain spectroscopy, " Physics in Medicine Biology, vol. 47, no. 21, pp. 413– 417 (2002).

C. Yu, S. Fan. Y. Sun, E. Pickwell-MacPherson, “The potential of terahertz imaging for cancer diagnosis: A review of investigations to date,” Quantitative Imaging in Medicine and Surgery, vol. 2, no. 1, pp. 33–45 (2012).

[45] https://www.umass.edu/cphm/content/real-time-breast-cancer-celldetection-terahertz.

[46] H. Cheon, H. J. Yang and J. H. Son, “Toward clinical cancer imaging using terahertz spectroscopy,” Journal of Selected Topics in Quantum Electronics, vol. 23, no. 4, pp. 1–9 (2017).

[47] K. I. Zaytsev, K. G. Kudrin, S. A. Koroleva, I. N. Fokina, S. I. Volodarskaya, E. V. Novitskaya, A. N. Perov, V. E. Karasik and S. O. Yurchenko, “Medical diagnostics using terahertz pulsed spectroscopy, ” J. Phys. Conf. Ser, vol. 486, no. 1, 012014 (2014).

[48] http://www.abc.net.au/news/2014-05-27/skin-cancer-laser-detection-toreduce-need-for-biopsies/5482004.

A. M. R. Pinto and M. Lopez-Amo, “Photonic crystal fibers for sensing applications, ” Journal of Sensors, vol. 2012, 598178 (2012).

[49] M. S. Islam, S. Rana, M. R. Islam, M. Faisal, H. Rahman, and J. Sultana, “Porous core photonic crystal fiber for ultra-low material loss in THz regime,” IET Communications, vol. 10, no. 16, pp. 2179–2183 (2016).

[50] J. Sultana, Md. S. Islam, J. Atai, M. R. Islam and D. Abbott “Nearzero dispersion flattened, low-loss porous-core waveguide design for terahertz signal transmission,” Opt. Eng., vol. 56, no. 7, 076114 (2017).

[51] Md. S. Islam, J. Sultana, J. Atai, M. R. Islam and D. Abbott,“Design and characterization of a low-loss, dispersion-flattened photonic crystal fiber for terahertz wave propagation,” Optik - International Journal for Light and Electron Optics., vol. 145, pp. 398–406 (2017).

[52] S. Islam, M. R. Islam, M. Faisal, A. S. M. S. Arefin, H. Rahman, J. Sultana, and S. Rana, “Extremely low-loss, dispersion flattened porous-core photonic crystal fiber for terahertz regime,” Optical Engineering., vol. 55, no. 7, 076117 (2016).

[53] M. S. Islam, J. Sultana, J. Atai, D. Abbott, S. Rana, and M. R. Islam, “Ultra low loss hybrid core porous fiber for broadband applications,”˜ Applied Optics., vol. 56, no. 4, pp. 1232–1237 (2017).

[54] M. S. Islam, J. Sultana, S. Rana, M. R. Islam, M. Faisal, S. F. Kaijage, and D. Abbott “Extremely low material loss and dispersion flattened TOPAS based circular porous

fiber for long distance terahertz wave transmission," Optical Fiber Technol., vol. 24, pp. 6–11 (2016).

A. M. Cubillas, S. Unterkofler, T. G. Euser, B. J. M. Etzold, A. C. Jones, P. J. Sadler, P. Wasserscheid, P. St. J. Russell, "Photonic crystal fibres for chemical sensing and photochemistry," Chem. Soc. Rev. , vol. 42, pp. 8629–8648 (2013).

B. M. B. Cordeiro, M. A. R. Franco, G. Chesini, E. C. S. Barretto, R. Lwin, C. H. B. Cruz, and M. C. J. Large "Microstructured-core optical fibre for evanescent sensing applications," Opt. Express, vol. 14, no. 26, pp. 13056–13066 (2006).

[55] Y. L. Hoo, W. Jin, H. L. Ho, D. N. Wang, R. S. Windeler, "Evanescentwave gas sensing using microstructure fiber" Optical Eng, vol. 41, no. 1, pp. 8–9 (2002).

[56] T. Kiwa, J. Kondo, S. Oka, I. Kawayama, H. Yamada, M. Tonouchi, and K. Tsukada, "Chemical sensing plate with a laser-terahertz monitoring system," Appl. Opt., vol. 47, no. 18, pp. 3324–3327 (2008).

[57] T. M. Monro, W. Belardi, K. Furusawa, J. C. Baggett, N. G. R. Broderick and D. J. Richardson, "Sensing with microstructured optical fibres," Measurement Science and Technology., vol. 12, no. 7, 854 (2001).

[58] Y. Yu, X. Li, X. Hong, Y. Deng, K. Song, Y. Geng, H. Wei, W. Tong, "Some features of the photonic crystal fiber temperature sensor with liquid ethanol filling," Opt. Express, vol. 18, no. 15, pp. 15383–15388 (2010).

[59] K. Lee, S. A. Asher, "Photonic crystal chemical sensors: pH and ionic strength," J. Am. Chem. Soc., vol. 122, no. 39, pp. 9534–9537 (2000).

[60] H. Ademgil "Highly sensitive octagonal photonic crystal fiber based sensor" Optik - International Journal for Light and Electron Optics., vol. 125, no. 20, pp. 6274–6278 (2014).

[61] H. Ademgil, and S. Haxha "Highly PCF based sensor with high sensitivity, high birefringence and low confinement losses for liquid analyte sensing applications," Sensors, vol. 15, no. 12, pp. 31833–31842 (2015).

[62] Md. F. H. Arif, K. Ahmed, S. Asaduzzaman, Md. A. K. Azad, "Design and optimization of photonic crystal fiber for liquid sensing applications," Photonic Sensors, vol. 6, no. 3, pp. 279–288 (2016).

[63] B. K. Paul, Md. S. Islam, K. Ahmed, S. Asaduzzaman, "Alcohol sensing over O+E+S+C+L+U transmission band based on porous cored octagonal photonic crystal fiber," Photonic Sensors, vol. 7, no. 2, pp. 123–130 (2017).

[64] S. Asaduzzaman, and K. Ahmed. "Microarray-Core Based Circular Photonic Crystal Fiber for High Chemical Sensing Capacity with Low Confinement Loss," Optica Applicata, vol. 47, no. 1, pp. 41–49 (2017).

[65] B. K. Paul, K. Ahmed, S. Asaduzzaman, Md. S. Islam, "Folded cladding porous shaped photonic crystal fiber with high sensitivity in optical sensing applications: design and analysis," Sensing and BioSensing Research,, vol. 12, pp. 36–42 (2017).

[66] M. Sharma, N. Borogohain, S. Konar, "Index guiding photonic crystal fibers with large birefringence and walk-off," J. Lightwave Technol., vol. 31, no. 21, pp. 3339–3344 (2013).

[67] S. E Kim, B. H. Kim, C. G. Lee, S. Lee, K. Oh, C. S. Kee, "Elliptical defected core photoniccrystal fiber with high birefringence and negative flattened dispersion, " Opt. Express., vol. 20, no. 2, pp. 1385–1391 (2012).

[68] Y. Y. Wang, N. V. Wheeler, F. Couny, P. J. Roberts, and F. Benabi, "Low loss broadband transmission in hypocycloid-core Kagome hollow-core photonic crystal fiber, " Opt. Lett., vol. 36, no. 5, pp. 669–671 (2011).

A. Hossain and Y. Namihira, "Light source design using Kagome lattice hollow core photonic crystal fibers, " Opt. Rev., vol. 21, no. 5, pp. 490– 495 (2014).

[69] http://www.topas.com/tech-center/performance-data/optics.

[70] T. M. Monro, W. Belardi, K. J. Furusawa, C. N. Baggett, G. R. Broderick, D. J. Richardson, "Sensing with microstructured optical fibres" Meas. Sci. Technol., vol. 12, pp. 854–858 (2011).

[71] B. T. Kuhlmey, B. J. Eggleton, and D. K. C. Wu, "Fluid-filled solidcore photonic bandgap fibers," J. Lightwave Technol., vol. 27, no. 11, pp. 1617–1630 (2008).

[72] M. Vieweg, T. Gissibl, S. Pricking, B. T. Kuhlmey, D. C.Wu, B. J. Eggleton, H. Giessen, "Ultrafast nonlinear optofluidics in selectively liquid-filled photonic crystal fibers," Opt. Express, vol. 18, no. 24, pp. 25232–25240 (2010).

[73] https://www.aao.org/eye-health/treatments/what-is-opticalcoherence-tomography.

[74] S. Chowdhury, S. Sen, K. Ahmed, S. Asaduzzaman, "Design of highly sensible porous shaped photonic crystal fiber with strong confinement field for optical sensing," Optik - International Journal for Light and Electron Optics, vol. 142, pp. 541–549 (2017).

[75] W. J. Wadsworth and R. M. Percival and G. Bouwmans and J. C. Knight and T. A. Birks and T. D. Hedley and P. S. J. Russell, “Very high numerical aperture fibers,” IEEE Photonics Technol. Lett., vol. 16, no. 3, pp. 843–845 (2004).

[76] S. Rana, A. S. Rakin, H. Subbaraman, R. Leonhardt and D. Abbott, “Low Loss and Low Dispersion Fiber for Transmission Applications in the Terahertz Regime,” IEEE Photonics Technol. Lett., vol. 29, no. 10, pp. 830–833 (2017).

[77] S. Atakaramians, S. Afshar, H. Ebendorff-Heidepriem, M. Nagel, B. M. Fischer, D. Abbott, and T. M. Monro, “THz porous fibers: design, fabrication and experimental characterization,” Opt. Express, vol. 17, no. 16, pp. 14053–14062 (2009).

[78] Fabrications of Photonic Crystal Fibers, Photonic Crystal Fibre Science, accessed on 12th September, 2017 [Online]. Available: http://www.mpl.mpg.de/en/russell/research/topics/fabrication.html.

A. M. Cubillas, S. Unterkofler, T.G. Euser, B. J. M. Etzold, A. C. Jones, P. J. Sadler, P. Wasserscheid, P. St. J. Russell, “Photonic crystal fibres for chemical sensing and photochemistry,” Chem. Soc. Rev., vol. 42, no.22, pp. 8629–8648 (2013).